

See discussions, stats, and author profiles for this publication at: <https://www.researchgate.net/publication/51495219>

Electrohydrodynamics of Soft Polyelectrolyte Multilayers: Point of Zero-Streaming Current

ARTICLE *in* LANGMUIR · AUGUST 2011

Impact Factor: 4.46 · DOI: 10.1021/la202292k · Source: PubMed

CITATIONS

26

READS

62

4 AUTHORS, INCLUDING:



[Jerome F.L. Duval](#)

French National Centre for Scientific Research

111 PUBLICATIONS **1,940** CITATIONS

[SEE PROFILE](#)



[Carsten Werner](#)

Leibniz Institute of Polymer Research Dresden

451 PUBLICATIONS **9,182** CITATIONS

[SEE PROFILE](#)

Electrohydrodynamics of Soft Polyelectrolyte Multilayers: Point of Zero-Streaming Current

Jérôme F. L. Duval,^{*,†} David Küttner,[‡] Carsten Werner,^{‡,§} and Ralf Zimmermann[‡]

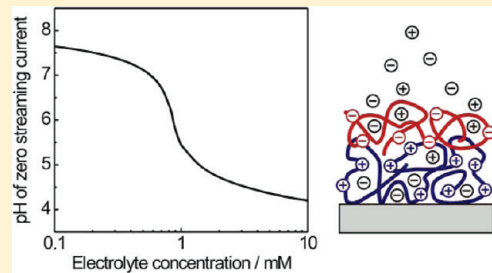
[†]Laboratoire Environnement et Minéralurgie, Nancy Université, CNRS UMR 7569, 15 avenue du Charmois, B.P. 40, 54501 Vandoeuvre-lès-Nancy, cedex France

[‡]Max Bergmann Center of Biomaterials Dresden, Leibniz Institute of Polymer Research Dresden, Hohe Strasse 6, 01069 Dresden, Germany

[§]Institute of Biomaterials and Biomedical Engineering, University of Toronto, 5 King's College Road, Toronto, Ontario, Canada M5S 3G8

 Supporting Information

ABSTRACT: We report a comprehensive formalism for the electrokinetics (streaming current, I_{str}) at soft multilayered polyelectrolyte films. These assemblies generally consist of a succession of permeable diffuse layers that differ in charge density, thickness, and hydrodynamic softness. The model, which extends one that we recently reported for the electrokinetics of monolayered soft thin films (Langmuir 2010, 26, 18169–18181), is valid without any restriction in the number and thickness of layers, or in the degree of dissociation and density of ionizable groups they carry. It further covers the limiting cases of hard and free draining films and correctly compares to semianalytical expressions derived for I_{str} under conditions where the Debye–Hückel approximation applies. The flexibility of the theory is illustrated by simulations of I_{str} for a two-layer assembly of cationic and anionic polymers over a large range of pH values and electrolyte concentrations. On this basis, it is shown that the point of zero streaming current (PZSC) of soft multilayered interphases, defined by the pH value where $I_{\text{str}} = 0$, generally depends on the concentration of the (indifferent) electrolyte. The magnitude and direction of the shift in PZSC with varying salinity are intrinsically governed by the dissymmetry in protolytic characteristics and density of dissociable groups within each layer constituting the film, together with the respective film thickness and hydrodynamic softness. The fundamental effects covered by the theory are illustrated by streaming current measurements performed on two practically relevant systems, a polyelectrolyte bilayer prepared from poly(ethylene imine) (PEI) and poly(acrylic acid) (PAA) and a polymer-cushioned (PEI) bilayer lipid membrane.



1. INTRODUCTION

During the past several decades, numerous strategies have been developed for the surface modification of bulk materials. Within the variety of chemical and physical approaches adopted for that purpose, particular emphasis has been placed on modification of surfaces by means of polymers. These approaches take advantage of the broad spectrum of polymer properties and options for polymer immobilization at surfaces to tailor the surface properties of bulk materials. A versatile and frequently used technique is the alternate physisorption of polycations and polyanions onto planar or colloidal supports.^{1–7} Providing that each deposition step leads to charge overcompensation at the surface, the process ultimately results in the generation of a polyelectrolyte multilayer (PEM).² Such a PEM can consist of successively deposited molecules and nano-objects of opposite charge, including linear and branched polymers, polypeptides, proteins, DNA, clay minerals, or carbon nanotubes.^{3,7} The variety of building blocks available for the assembly of PEMs and the further option to combine the layer-by-layer fabrication process with other assembly procedures, make PEMs attractive for a broad range of applications,³ such as drug

delivery,⁸ antimicrobial coatings,⁹ ion-selective membranes,¹⁰ protein-selective surfaces,¹¹ biosensors,¹² and stimuli-responsive thin films.¹³

The optimization of PEM performance within the framework of these applications necessarily requires fundamental knowledge of the physicochemical properties of PEMs, including their growth, swellability, stability, and structure, as well as their control during the assembly process.² This necessarily includes analyses of the charge/electric double layer formation, the screening and interaction of the sublayers in an aqueous environment, the formation of salt bridges, and the processes underlying the impact of charge on PEM structure. It is now well-established that measurements of streaming potential/current and surface conductivity are appropriate to achieve such a degree of understanding. Advanced theories are now available for adequate physical interpretation of electrokinetic data collected at

Received: June 18, 2011

Revised: July 14, 2011

Published: July 15, 2011

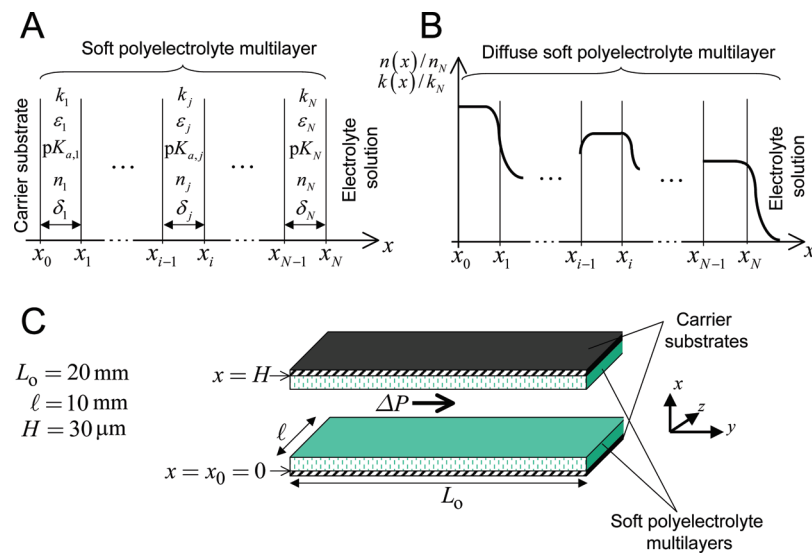


Figure 1. (A) Schematic representation of a soft multilayered film. The figure details the nomenclature adopted in the theory of section 2, in particular, that used for modeling the protolytic features of each layer constituting the film. (B) Schematic drawing of the situation where the distribution $n(x)$ of the concentration of ionizable sites from the carrier surface to the outer solution and the distribution of the friction $k(x)$ exerted by the film on the flow are described by a continuous function with a smooth transition between adjacent layers. The progressivity of the transitions is ruled by the parameters α_j . (C) Details of the microslit cell used for electrokinetic experiments.

polymer/solution interfaces,^{14–23} which are paradigms of soft (permeable) interphases. The analysis requires abandoning the classical concept of zeta potential and, instead, necessitates the account of fluid penetration within the electrokinetically active zone of the polymer material under lateral flow conditions.^{19,20,22–24} Following such a strategy, it is now possible to unambiguously unravel the electrostatic, hydrodynamic, and structural properties of materials such as micrometer-thick hydrogels,^{19,20,25} uncharged thermoresponsive thin films,²² and ionic-strength-/pH-responsive thin polymer coatings.²³

Surprisingly, despite the aforementioned importance of soft PEM materials in a number of biomedical and environmental applications, no theory is available for capturing the basics of their electrokinetic properties under lateral pressure-driven flow conditions. This is essentially the purpose of this work, which extends our previous formalism developed strictly for the electrokinetics of monolayered diffuse (heterogeneous) soft films.^{22,23} A numerical analysis of the governing electrokinetic equations is reported for evaluating the streaming current within the most general situation of a PEM that consists of N ($N \geq 1$) charged layers of given thickness, hydrodynamic softness, and charge density. The formalism is valid without any limitation on the degree of dissociation for the ionizable groups carried by the various layers. It is further applicable for any spatial distribution of charge and soft material density (diffuse PEM interphase) without restriction on the magnitude of the charge densities and thicknesses of the layers. Semianalytical expressions for the streaming current are further provided within the Debye–Hückel approximation.

This article is organized as follows: The theory is first developed, and the typical electrokinetic properties of PEMs are then discussed on the basis of illustrative simulations given for a two-layer assembly of cationic and anionic polymers. In particular, it is demonstrated how the charge, thickness, and hydrodynamic softness of the internal layer affect the ionic strength and pH dependence of the streaming current of the

PEM. We demonstrate that the pH value defining the condition of zero streaming current for the PEM depends on indifferent electrolyte concentration and is further impacted by the relevant electrostatic and hydrodynamic properties of each layer constituting the PEM. In a second part, streaming current data collected for a poly(ethylene imine) (PEI)/poly(acrylic acid) (PAA) bilayer over a large range of KCl concentrations (0.1–10 mM) and pH values (3–9) are shown to support the electrolyte concentration dependence of the PZSC as anticipated from theory. A second set of streaming current data obtained for a polymer-cushioned (PEI) bilayer lipid membrane further underlines the relevance of our theoretical approach for tackling electrokinetics of complex chemically stratified soft materials that are ubiquitous in such fields as biology and environmental science.

2. THEORY

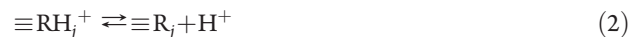
2.1. Problem Description. In the following discussion, we derive the electrokinetic properties of a soft polyelectrolyte multilayer (PEM) in an electrolyte solution containing M ions of valency z_i and bulk concentration c_i with $i = 1, \dots, M$. The nomenclature adopted below conforms to that of Duval et al. in their recent theory for the electrostatic interactions between PEMs carried by spherical colloids or planar surfaces.²⁶ In detail, the PEM is composed of N successive layers to which we assign the index j , with $j = 1$ referring to the most internal layer, that is, that supported by the hard substrate, and $j = N$ referring to the layer located in the direct vicinity of the external electrolyte solution (Figure 1A). The thickness of layer j , $j = 1, \dots, N$, is denoted as δ_j . We position the N layers with the space variable x that refers to the dimension perpendicular to the PEM/electrolyte solution interphase. x runs from $x_0 = 0$ to $x_N = \sum_{j=1}^N \delta_j$, which correspond to the position of the carrier surface and that of the interphase formed between the N th layer and the solution, respectively. The theory includes the possibility of heterogeneous (diffuse) distribution for the density of charge

and soft material across the PEM (Figure 1B), as further detailed in sections 2.1.1 and 2.1.2, respectively. For the electrokinetic measurements, two soft surface PEMs are positioned in a cell with the experimental arrangements shown schematically in Figure 1C. Under the action of an externally applied pressure drop ΔP across the channel (y direction), a streaming current I_{str} arises as a result of displacement of mobile electrolyte ions distributed in the PEM electric double layer that extends from the carrier surface to the bulk electrolyte solution. In line with situations of practical interest, the theory is developed for the laminar flow regime and steady-state hydrodynamic and electrostatic fields across the PEM. In addition, it applies to cases in which the soft (possibly diffuse) surface layers within the cell and their electric double layers do not overlap, that is, $H \gg 2\sum_{j=1}^N \delta_j$ and $\kappa H \gg 2$, where H is the height of the electrokinetic channel and κ the reciprocal Debye length (Figure 1C). It further disregards edge effects, which are negligible for the typical dimensions of cells used in the experiments (Figure 1C). For the sake of readability, each layer within the PEM is further assumed to contain a single type of dissociable groups. Straightforward modifications of the formalism along the lines detailed in refs 27 and 28 for the electrophoresis of soft multilayered (bio)colloids can be made to include the presence of groups of different natures within a given layer of the PEM. In the following model development, we consider that the PEM electrostatic and hydrodynamic properties (i.e., the distribution of charges and local friction, respectively) are invariant by translation along the y direction. In turn, the problem is one-dimensional, with the electric and flow velocity fields depending on only the relevant position x across the film. In addition, we adopt a smeared-out approach for modeling the x -dependent distribution of charges within the film. Such a method is adequate providing that the Debye layer thickness well exceeds the typical separation distance between neighboring functional groups. Finally, various complex processes that likely occur within the PEM are not explicitly included in the theory. Among them, the very dependence of the thickness of the charged layers composing the PEM on pH and electrolyte concentration (swelling/shrinking processes) is not considered. Such analysis is beyond the scope of the current theory that poses the basis of PEM electrokinetics. It would require a cautious determination of the steady-state thickness of each layer, as governed by a local balance between elastic, entropic (polymer-mixing), and electrostatic contributions to osmotic pressure. In this respect, we do not explicitly account for the physical mechanisms leading to possible interpenetration of the various film layers, which can result in the formation of salt bridges and in the local screening of charges. Again, evaluation of such mechanisms necessitates inclusion in the theory of the local elasticity of the PEM chains within the constituting layers, together with their propensity to extend/retract upon action of local electric field gradients within the film.

2.1.1. Distribution Profile for the Density of Fixed (Immobile) Charges across the PEM. The charge density carried by a given layer j is assumed to originate either from the deprotonation of basic groups (e.g., amino groups), denoted $\equiv\text{RH}_{j=1,\dots,M}^+$, or from the deprotonation of acid groups (e.g., carboxylic groups), $\equiv\text{RH}_{j=1,\dots,M}$, according to the charging mechanisms



and



where $\equiv\text{R}$ refers to the polymeric material within layer j . To specify the type of reaction relevant for a given layer j , we set $\varepsilon_j = -1$ when eq 1 applies and $\varepsilon_j = +1$ for the other case in which eq 2 adequately depicts the origin of the charge. The acidity constant associated with the relevant acid–base reaction taking place in the j th layer is then denoted as $K_{\text{a},j} = 10^{-\text{p}K_{\text{a},j}}$. The volume concentration of ionizable groups $\equiv\text{R}$ within the j th layer is called n_j . Within this representation of the PEM, the profile for the concentration of ionizable groups, $n(x_0 < x < x_N)$, consists of a succession of discontinuous square functions of amplitude n_j . To integrate the possibility of a smooth transition for $n(x)$ across the PEM/electrolyte solution interphase, we adopt the expression given by Duval et al.²⁶

$$x \geq x_0 \quad n(x) = \chi \left[\sum_{j=1}^{N-1} (n_j - n_{j+1})f_j(x) + n_N f_N(x) \right] \quad (3)$$

with

$$f_{j=1,\dots,N}(x) = \frac{1}{2} \left\{ 1 - \tanh \left[\left(x - x_0 - \sum_{k=1}^j \delta_k \right) / \alpha_j \right] \right\} \quad (4)$$

which extends the representation of monolayered soft diffuse interphases^{22,23} to the general case of soft diffuse PEMs. It is stressed that the spatial profile $n(x)$ given by eqs 3 and 4 is continuous for any position $x \geq x_0$. The gradual variation of $n(x)$ between two adjacent layers j and $j + 1$ is governed by the quantities α_j (Figure 1B).²⁶ In the limit $\alpha_j \rightarrow 0$, eqs 3 and 4 reduce to a succession of step functions. To ensure that the total amount of ionizable sites, or equivalently the total amount of polymer segments within the PEM, remains constant upon modification of the profile $n(x)$ (i.e., variation in α_j), we define the constant χ in eq 3 according to the expression^{22,26}

$$\chi = \sum_{j=1}^N n_j \delta_j / \int_{x_0}^{\infty} \left[\sum_{j=1}^{N-1} (n_j - n_{j+1})f_j(x) + n_N f_N(x) \right] dx \quad (5)$$

The local density of fixed charges at a given position x , denoted as ρ_{fix} , depends on the corresponding local concentration of ionizable sites, $n(x)$ (eqs 3–5), on the local dimensionless electrostatic potential $y(x)$ [$y(x) = F\psi(x)/RT$, with T the absolute temperature, R the gas constant, ψ the potential, and F the Faraday constant], on the solution pH, and on the nature of the acid–base equilibrium that applies at this position. For the acid–base reactions detailed in eqs 1 and 2, we obtain²⁶

$$x \geq x_0 \quad \rho_{\text{fix}}(x, y) = \chi \rho_N \left\{ \sum_{j=1}^{N-1} [\gamma_{j,N} \mu_j(y) - \gamma_{j+1,N} \mu_{j+1}(y)] f_j(x) + \mu_N(y) f_N(x) \right\} \quad (6)$$

The dimensionless factors $\gamma_{j,N}$ introduced in eq 6 are given by $\gamma_{j,N} = \rho_j / \rho_N$, where the quantities $\rho_j = F\varepsilon_j n_j$ represent the maximum charge density reachable within layer j in the limits

where ionizable groups are uniformly distributed in the layer and completely dissociated. In eq 6, the partial dissociation functions $\mu_j(y)$ for the ionizable groups located at position x within the j th layer are provided by classical Langmuir isotherms corrected for electrostatics

$$\mu_j(y) = [1 + 10^{-\varepsilon_j(pK_j - pH)} \exp(\varepsilon_j y)]^{-1} \quad (7)$$

For a given layer j , complete dissociation of ionizable groups is reached at any position $x_j \leq x \leq x_{j+1}$ provided that the condition $\mu_j(y) \rightarrow 1$, or equivalently $\varepsilon_j(pK_j - pH) \gg 1$, is satisfied.

2.1.2. Distribution Profile for the Hydrodynamic Softness across the PEM. In the limit $\alpha_j \rightarrow 0$ where the PEM consists of uniform soft layers of polymer segment density n_j^s and volume concentration n_j of ionizable groups, we rationalize the friction exerted on the flow by layer j using the Debye–Bueche formalism for hydrodynamics in porous media.²⁴ Within this representation, where each layer is assimilated to a set of resistance centers of radius a_j^s , the friction coefficient pertaining to layer j is given, under conditions of sufficiently high water content, by $k_j = 9\eta\phi_j(a_j^s)^{-2}/2$, where η is the dynamic fluid viscosity and $\phi_j = 4\pi n_j^s (a_j^s)^3/3$ is the hydrodynamic volume fraction of polymer segments located in the j th layer. As is commonly done within the framework of soft surface electrokinetic modeling,^{23–25,27,29,30} we further assign to each layer j a hydrodynamic softness, $\lambda_j = (k_j/\eta)^{1/2}$, where the quantity $1/\lambda_j$ has the dimension of a length that characterizes the typical degree of fluid flow penetration within the j th layer. Assuming that the concentration of ionizable groups across the various layers composing the PEM is linearly related to the density of polymer segments therein,^{19,20,22,23,25,27,30} for a soft diffuse PEM/solution interphase, we obtain the following distribution of the friction coefficient $k(x)$

$$x \geq x_0 \quad k(x) = \chi k_N \left[\sum_{j=1}^{N-1} (\omega_{j,N} - \omega_{j+1,N}) f_j(x) + f_N(x) \right] \quad (8)$$

where the dimensionless quantity $\omega_{j,N} = k_j/k_N = (\lambda_j/\lambda_N)^2$ reflects the degree of hydrodynamic softness of layer j as compared to that of the most external PEM layer ($j = N$), which directly faces the electrolyte solution.

2.2. Electrostatic and Hydrodynamic Fields across the PEM/Solution Interphase, Evaluation of Streaming Current. *Electrostatics.* Reasoning along the lines set forth in our previous modeling of electrohydrodynamics of soft diffuse monolayered interphases,^{22,23} the distribution of the electrostatic potential y across the PEM is provided by the nonlinear Poisson–Boltzmann equation, which includes the charge density term stemming from mobile electrolyte ions distributed inside and outside the PEM, as well as the term that originates from the ionizable groups it carries

$$\frac{d^2y(X)}{dX^2} = -(\kappa H)^2 \left\{ \sum_{i=1}^M z_i c_i \exp[-z_i y(X)] + \rho_{\text{fix}}(X, y)/F \right\} / \sum_{i=1}^M c_i z_i^2 \quad (9)$$

where $X = x/H$ is the dimensionless space variable and H is the height of the electrokinetic channel (Figure 1C). The quantity $\rho_{\text{fix}}(X, y)$ involved in eq 9 is defined by eq 6, and κ represents the reciprocal Debye thickness $\kappa = [\sum_{i=1}^M F^2 c_i z_i^2 / (\epsilon_0 \epsilon_r RT)]^{1/2}$, where $\epsilon_0 \epsilon_r$ is the solution dielectric permittivity, which is assumed to be identical to that of the film (valid for sufficiently high water

content within the PEM). The boundaries associated with eq 9 are given by $dy/dX|_{X=x_0/H} = 0$ and $y(X \rightarrow 1/2) \rightarrow 0$.^{22,23} The former indicates the overcompensation of the charge at the substrate surface after the adsorption of the first layer (i.e., the charge of the first layer is assumed to be much higher than the substrate charge), and the latter defines the bulk reference for the potential. Relaxing the condition of no substrate charge is straightforward; see details in ref 23.

Hydrodynamics. The hydrodynamic flow field velocity is oriented parallel to the substrate/PEM. Its magnitude, denoted as v , depends on the position x according to the Brinkman equation²⁴

$$\frac{d^2V(X)}{dX^2} - [\lambda(X)H]^2 V(X) = -1 \quad (10)$$

where $V(X)$ is the dimensionless flow velocity $V(X) = v(X)/[\Delta PH^2 / (\eta L_o)]$ and $\lambda(X)$ the local hydrodynamic softness related to the local friction coefficient $k(X)$ (eq 8) through $\lambda(X) = [k(X)/\eta]^{1/2}$. The boundaries pertaining to eq 10 reflect the no-slip conditions at the carrier surface [$V(X = x_0/H) = 0$] and the symmetry of the problem with respect to the position $X = 1/2$ [$dV(X)/dX|_{X=1/2} = 0$].^{22,23}

Electrokinetics. Given the distribution profiles for the fields of potential $y(X)$ and flow velocity $V(X)$, the streaming current I_{str} of the PEM is defined by²³

$$I_{\text{str}}/\Delta P = \frac{2lFH^3}{\eta L_o} \int_0^{1/2} V(X) \sum_{i=1}^M z_i c_i \exp[-z_i y(X)] dX \quad (11)$$

where l and L_o are the width and length, respectively, of the electrokinetic channel (Figure 1C). In addition, we define the point of zero streaming current, hereafter denoted as PZSC, as the pH value where $I_{\text{str}} = 0$, that is

$$\text{PZSC} = \text{pH}|_{I_{\text{str}}=0} \quad (12)$$

As extensively discussed in section 3, the PZSC is a key parameter for understanding and characterizing the electrohydrodynamic properties of PEMs because it directly reflects the subtle balance between the electrostatic potential distribution and flow velocity field developed within the film, where this balance is impacted by the electrolyte composition (i.e., salt content and pH) and by the structure of the constituting film layers (thickness, nature of local charges, local friction properties). It is emphasized here that streaming current and streaming potential are linearly related by Ohm's law, where a positive surface conductivity term is involved. As a consequence, the PZSC for chemically stratified thin films, as extensively analyzed in the following sections, identifies to the point of zero streaming potential (PZSP). It is recalled that the measurement of either streaming potential or streaming current depends on the arrangement of the electrokinetic cell, where the former corresponds to zero overall current and the latter to zero potential drop across the channel in the stationary state.

2.3. Numerical Solution. The distributions of the electrostatic potential $y(X)$ and pressure-driven flow velocity $V(X)$ across the PEM were obtained by numerical evaluation (with appropriate boundaries as specified in section 2.2) of differential eqs 9 and 10, respectively, according to a methodology described in details elsewhere.^{22,23} We verified that the numerical code used in the limit $N = 1$ provides the profiles $y(X)$ and $V(X)$ and the

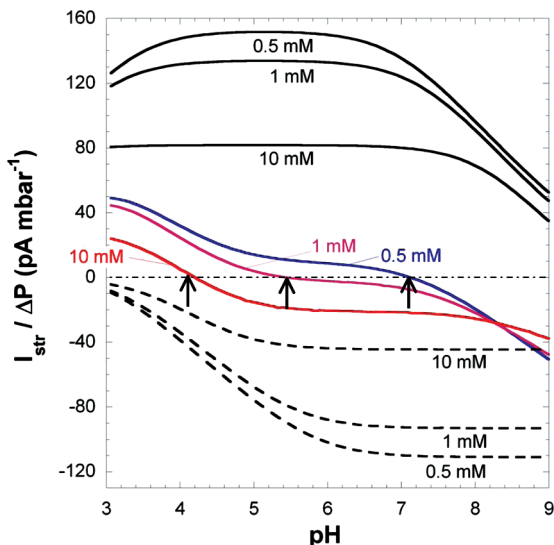


Figure 2. Ratio between streaming current (I_{str}) and applied pressure (ΔP) as a function of pH as evaluated at three electrolyte concentrations (indicated) for a polycationic layer (black solid lines), a polyanionic layer (black dashed lines), and a polycation ($j = 1$)/polyanion ($j = 2$) bilayer film (colored lines). Model parameters for the bilayer system: $pK_{a,1} = 9$, $\varepsilon_1 = +1$, $\delta_1 = 30 \text{ nm}$, $pK_{a,2} = 4$, $\varepsilon_2 = -1$, $\delta_2 = 5 \text{ nm}$, $n_2 = 20 \text{ mM}$, $1/\lambda_2 = 4.5 \text{ nm}$, $|\gamma_{1,2}| = 1$, $\omega_{1,2} = 1$, and $\alpha_{j=1,2} \rightarrow 0$. Model parameters for the polycation layer and polyanion layer are similar to those adopted for the polycationic and polyanionic layers forming the bilayer film. Arrows highlight the decrease of the PZSC for the bilayer film with increasing electrolyte concentration.

corresponding value I_{str} as obtained from the theory reported in ref 23 for electrokinetics of monolayered soft films. In addition, the validity of the numerical code was addressed by comparison of exact numerical results for the streaming current of poorly charged and homogeneous PEMs, with analytical and semianalytical expressions derived in the Supporting Information for I_{str} in the limits $y(X) \ll 1$ (Debye–Hückel approximation) and $\alpha_{j=1,\dots,N} = 0$.

For the sake of demonstration, the basics of the electrokinetics of PEMs are mostly discussed here in the limit $\alpha_{j=1,\dots,N} \rightarrow 0$ (homogeneous PEM). The use of the spatial profiles defined by eqs 3 and 8 in this limit avoids the necessity of introducing boundary conditions other than those specified in section 2.2. Solving the governing electrostatic and hydrodynamic equations under the strict condition $\alpha_{j=1,\dots,N} = 0$ indeed requires the further tedious accounting of the continuity of the potential, electric field, velocity, and shear stress at positions $x = x_{j=1,\dots,N}$ (see details in the Supporting Information). The results are given at the end of section 3 to appreciate, for example, the effect of heterogeneity of the outermost layer (i.e., impact of $\alpha_{j=N}$) on the electrokinetics and point of zero streaming current for diffuse PEMs. Finally, it is emphasized that the surface conductivity of homogeneous or diffuse PEMs, which is an experimentally accessible quantity,²³ can be easily computed from the here-reported theory using eqs 10–13 in ref 23 and replacing there the term $(\lambda_o)^2 f(X)$ by $[\lambda(X)]^2$ as defined in section 2.2.

3. RESULTS AND DISCUSSION

To capture the fundamental electrokinetic properties of chemically stratified systems such as PEMs, the theoretical results

discussed in this section pertain to a two-layer assembly ($N = 2$) of cationic ($j = 1$) and anionic polymers ($j = 2$). If not otherwise specified in the text, the electrohydrodynamic parameters characterizing the layers are as follows: $pK_{a,1} = 9$, $\varepsilon_1 = +1$, $\delta_1 = 30 \text{ nm}$, $pK_{a,2} = 4$, $\varepsilon_2 = -1$, $\delta_2 = 5 \text{ nm}$, $n_2 = 20 \text{ mM}$, $1/\lambda_2 = 4.5 \text{ nm}$, $|\gamma_{1,2}| = 1$, $\omega_{1,2} = 1$, and $\alpha_{j=1,2} \rightarrow 0$. The considered electrolyte is monovalent and symmetric, and we denote the bulk concentration of electrolyte anions and cations in solution as c . Simulations are given for c in the range of 0.1 – 10 mM , which corresponds to concentrations typically used in streaming current measurements at varied solution pH values.^{22,23}

As a starting point, Figure 2 displays the dependence of the pressure-normalized streaming current, $I_{\text{str}}/\Delta P$, on pH for the bilayer system described above at three values of c (0.5 , 1 , and 10 mM). For the sake of comparison, the electrokinetic responses of the cationic and anionic layers taken separately are also given. The streaming currents for the monolayered anionic ($I_{\text{str}}/\Delta P < 0$) and cationic ($I_{\text{str}}/\Delta P > 0$) films exhibit a classical dependence on c and pH. At fixed pH, $|I_{\text{str}}/\Delta P|$ decreases with increasing c as a result of charge screening by ions in solution. For a given c , $|I_{\text{str}}/\Delta P|$ increases with decreasing pH for the cationic film, whereas an increase of $|I_{\text{str}}/\Delta P|$ is observed with increasing pH in the case of the anionic film. These trends are in line with the dissociation of ionizable groups as governed by the quantity $\varepsilon_j(pK_{a,j} - \text{pH})$ involved in the dissociation function $\mu_j(y)$ (eq 6). At sufficiently low pH and electrolyte concentration, the contribution of the protons to the overall solution ionic strength can lead to a significant compression of the electric double layer and, therefore, to a reduction of $|I_{\text{str}}/\Delta P|$, as observed for the cationic film. The electrokinetic properties of the cationic/anionic bilayer considerably differ from those of the layers constituting the film. Whereas, for a given c , the rate of variation of $|I_{\text{str}}/\Delta P|$ with pH is somehow reminiscent of that discussed for the cationic and anionic layers at high and low pH, respectively, the streaming current for the PEM exhibits the particular feature to vanish for a given pH value (see arrows in Figure 2), the point of zero streaming current (PZSC). The PZSC is obviously concentration-dependent and, under the conditions of Figure 2, is shifted to the left with increasing c . Figure 3A further shows that the PZSC is generally a function of the characteristic flow penetration length, $1/\lambda_2$, within layer 2.

3.1. Dependence of the Point of Zero Streaming Current (PZSC) on Electrolyte Concentration. To first understand the physical origin of the shift in PZSC with increasing c at fixed $1/\lambda_2$ (Figures 2 and 3A), we report in Figure 4A the potential and velocity profiles at $c = 0.1$, 1 , and 10 mM ; $1/\lambda_2 = 4.5 \text{ nm}$ [i.e., $1/(\lambda_2 \delta_2) = 0.9$]; and $\text{pH} \approx 5.45$ that corresponds to the PZSC in 1 mM electrolyte (indicated in Figure 3A). As c increases from 1 to 10 mM , the electric double layer is gradually located within the outermost region of the film in line with an increase of $\kappa \delta_2$. As a result, the local potential distribution at the very interphase formed between layer 2 and the solution increasingly reflects the protolytic characteristics of the functional groups distributed therein (in particular, $\varepsilon_2 = -1$). In turn, $y(x)$ becomes more negative in this region of the film despite the stronger screening that operates only in the bulk of the bilayer film, leading to a decrease of the Donnan potential. Because the modulations of the potential distribution following the increase of c spans over the film region that is most effectively probed by the flow (see the velocity distribution at 10 mM in Figure 4A), the conditions required for $I_{\text{str}}/\Delta P = 0$ are no longer satisfied at 10 mM electrolyte concentration. They are recovered with decreasing

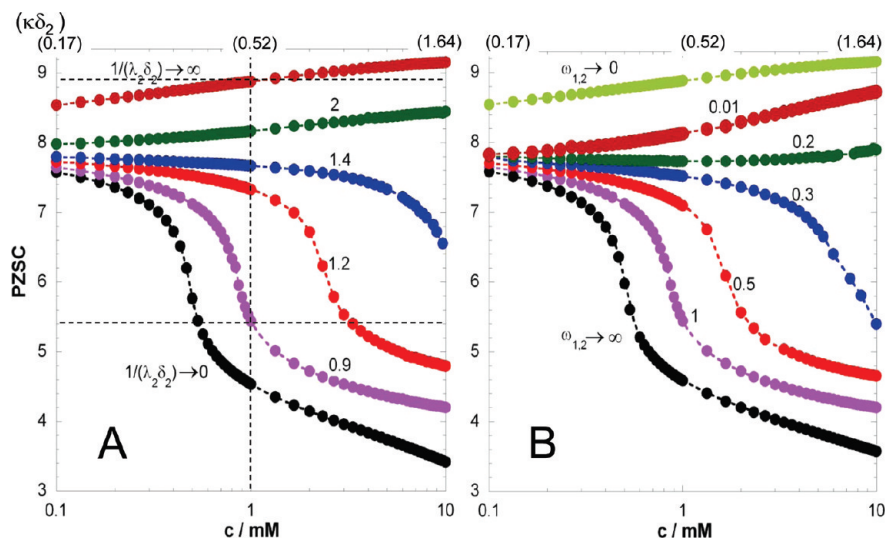


Figure 3. Point of zero streaming current (PZSC) versus electrolyte concentration for various values of (A) the hydrodynamic softness λ_2 [or equivalently $1/(\lambda_2\delta_2)$] and (B) the ratio $\omega_{1,2} = k_1/k_2 = (\lambda_1/\lambda_2)^2$ for a bilayer film. Other model parameters as in Figure 2. Dotted lines are guides to the eye. Horizontal and vertical dashed lines in panel A indicate pH values and electrolyte concentrations at which potential and velocity field distributions are given in Figure 4 (see text for details).

pH, that is, with decreasing number density of negatively charged groups in layer 2 (dotted line, Figure 4A, $c = 10 \text{ mM}$). This explains why the PZSC at 10 mM is lower than that at 1 mM for $1/\lambda_2 = 4.5 \text{ nm}$. As c decreases from 1 to 0.1 mM, the double layer now extends significantly within layer 1 following a significant decrease of $\kappa\delta_2$. Then, the potential distribution becomes mainly determined by the electrostatic features of the internal layer 1, which is manifested by the absence of a sign reversal in $y(x)$, which remains positive all across the bilayer at $c = 0.1 \text{ mM}$ (Figure 4A). To retrieve the PZSC condition, it is necessary to increase the pH significantly so as to force $y(x)$ to change sign across the film as a result of the increasing negative charge carried by layer 2 (dotted line, Figure 4A, $c = 0.1 \text{ mM}$). This concomitantly generates a decrease of the potential within layer 1 in line with a decrease of the amount of positive charge therein. The dependence of the PZSC on c at $1/(\lambda_2\delta_2) = 0.9$, as commented above from Figures 3A and 4A, further exhibits the particularity that, at sufficiently low and high values of $\kappa\delta_2$ (i.e., low and high electrolyte concentration c , Figure 3A), the rate of decrease of the PZSC with increasing c is less pronounced than that observed at intermediate $\kappa\delta_2$ and eventually tends asymptotically to zero. In these limits of thick and thin double layers ($\kappa\delta_2 \ll 1$ and $\kappa\delta_2 \gg 1$, respectively), the potential distribution $y(x)$ becomes predominantly governed either by the electrostatic features of the inner layer ($\kappa\delta_2 \ll 1$) or by those of the outermost layer ($\kappa\delta_2 \gg 1$) so that, in turn, the impact of c on the PZSC becomes significantly reduced.

3.2. Dependence of the Point of Zero Streaming Current (PZSC) on Flow Field Structure. The explanations given above for the sigmoid-like decrease of the PZSC with increasing c at $1/(\lambda_2\delta_2) = 0.9$ hold for $1/(\lambda_2\delta_2)$ values between 0 and 1.4 (Figure 3A). Quantitatively, we observe that the concentrations where this decrease of the PZSC is most significant are shifted to higher values as $1/(\lambda_2\delta_2)$ increases from 0 to 1.4. The reason for this behavior is illustrated in Figure 4B, where velocity profiles across the bilayer are given for various values of $1/(\lambda_2\delta_2)$ at fixed $c = 1 \text{ mM}$ and $\text{pH} \approx 5.45$. Let us start from the situation at $1/(\lambda_2\delta_2) = 0.9$, where the conditions required for $I_{\text{str}}/\Delta P = 0$ are

satisfied (Figure 3A). With decreasing $1/(\lambda_2\delta_2)$, penetration of the flow within the film is reduced (Figure 4B) or, stated differently, the thickness of the electrokinetically active zone of the film (that is, that where charge distribution is probed by the tangential flow) is decreased. In turn, $I_{\text{str}}/\Delta P$ becomes negative as a result of the increasing contribution of layer 2 in determining the electrokinetic properties of the film as a whole. To re-establish the condition in line with $I_{\text{str}}/\Delta P = 0$, it is necessary to increase the role played by layer 1. This is done with decreasing c or, equivalently, $\kappa\delta_2$, which, as commented in Figure 4A, results in a decrease (increase) within layer 2 (layer 1) of the local potential $|y(x)|$. Conversely, for increasing values of $1/(\lambda_2\delta_2)$ at fixed pH, the PZSC is met for increasing values of $\kappa\delta_2$, in agreement with results reported in Figure 3A.

For situations where $1/(\lambda_2\delta_2) \gg 1$, the friction exerted by the film on the flow is significantly reduced, and in the limit $1/(\lambda_2\delta_2) \rightarrow \infty$, the film becomes free-draining. From a hydrodynamic point of view, the presence of the film then becomes immaterial, and the velocity profile is identical to that given by the Poiseuille equation for a pressure-driven flow within a rectangular channel of height H (Figure 4C). Under such conditions, the PZSC is now increasing with increasing electrolyte concentration, as illustrated in Figure 3A. This change in the dependence of the PZSC on c as compared to cases of low to moderate $1/(\lambda_2\delta_2)$, is explained upon inspection of the flow and potential profiles depicted in Figure 4C at $c = 0.1, 1, 10 \text{ mM}$, $1/(\lambda_2\delta_2) \rightarrow \infty$, and $\text{pH} \approx 8.9$. The latter pH value corresponds to the PZSC at $c = 1 \text{ mM}$ when the film is free-draining (Figure 3A). As c increases from 1 to 10 mM, $|y(x)|$ decreases across the film as a result of double layer compression. Despite the increased contribution of layer 2 in determining $I_{\text{str}}/\Delta P$ with increasing c (or $\kappa\delta_2$), the overall electrokinetic response of the film remains predominantly determined by the electrostatic features of layer 1 in view of $1/(\lambda_2\delta_2) \rightarrow \infty$ and $\delta_1/\delta_2 \gg 1$. As a result, to recover the PZSC at 10 mM, it is necessary to increase the pH (dotted line in Figure 4C, $c = 10 \text{ mM}$) so as to decrease the magnitude of $|y(x)|$ within layer 1. This increase of pH hardly affects the potential distribution within layer 2 because, under the range of pH

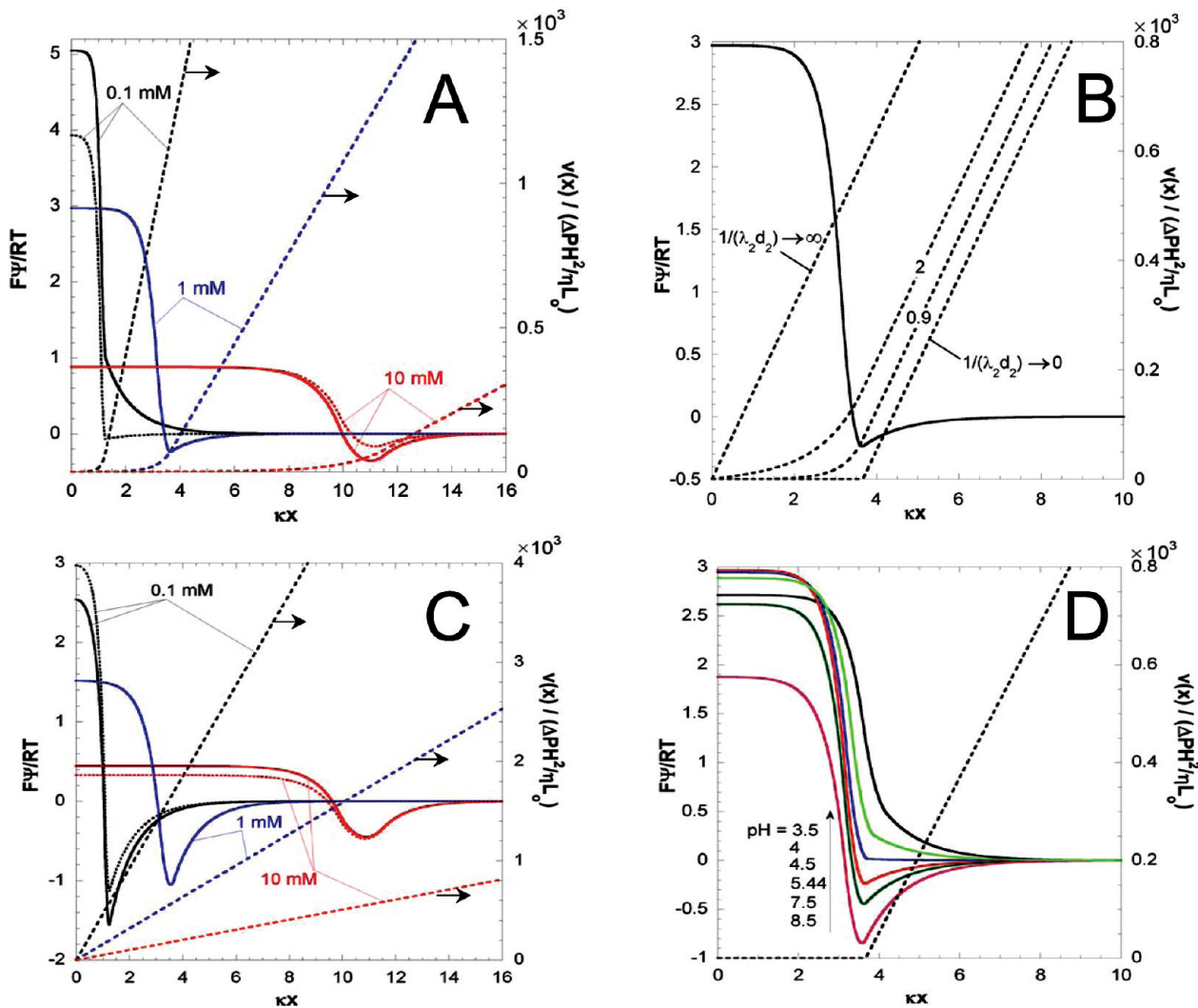


Figure 4. (A) Dimensionless electrostatic potential (colored solid and dotted lines) and velocity (colored dashed lines marked with arrows) across the bilayer film at 0.1, 1, and 10 mM electrolyte concentrations. Model parameters as in Figure 2, except pH = 5.45 (solid lines for the potential distribution in 0.1, 1, and 10 mM), pH = 4.22 (dotted line for the potential distribution at 10 mM), and pH = 7.64 (dotted line for the potential distribution at 0.1 mM). See further details in the main text. (B) Dimensionless electrostatic potential (solid line) and velocity field profiles (dotted lines) at various values of $1/(\lambda_2 \delta_2)$ (indicated) across a bilayer film. Model parameters as in Figure 2, with $c = 1$ mM, pH = 5.45. (C) As in panel A for $1/(\lambda_2 \delta_2) \rightarrow \infty$, pH = 8.88 (solid curves for the potential distribution at 0.1, 1, and 10 mM), pH = 9.15 (dotted line for the potential distribution at 10 mM), and pH = 8.54 (dotted line for the potential distribution at 0.1 mM). (D) Dimensionless electrostatic potential (solid colored lines) and velocity field [$1/(\lambda_2 \delta_2) \rightarrow 0$, dotted line] in 1 mM electrolyte concentration at various values of pH (indicated) across a bilayer film. Other model parameters as in Figure 2.

considered, dissociation of the charges carried by the outer layer of the film is complete, as judged from the dependence of $I_{\text{str}}/\Delta P$ on pH reported in Figure 2 for the anionic layer. Conversely, when decreasing the electrolyte concentration from 1 to 0.1 mM under the conditions $1/(\lambda_2 \delta_2) \rightarrow \infty$ and pH ≈ 8.9 , the situation of zero streaming current is retrieved by decreasing the pH to ~ 8.5 (Figures 3A and 4C).

In the limit $1/(\lambda_2 \delta_2) \rightarrow 0$, the PEM film is hard, and the streaming current is strictly determined by the flow of mobile ions located outside the film only. Making the analogy with the Smoluchowski formulation of streaming current for hard systems, we show that, for $1/(\lambda_2 \delta_2) \rightarrow 0$, $I_{\text{str}}/\Delta P$ is determined by the value of the electrostatic potential at the position $x = \sum_{j=1}^2 \delta_j$. The PZSC then corresponds to the pH value where the outer potential of the film is zero (Figure 4D). As such, it identifies to the isoelectric point (IEP) classically introduced in electrokinetic

theory of hard systems. For impermeable and permeable PEMs, the net charge of the multilayered film as a whole is not necessarily zero at the IEP, however, as recognized long ago by Ohshima in his derivation of IEP for ion-permeable but flow-impermeable membranes consisting of a cationic and anionic layer under Donnan conditions.¹⁷ The trend discussed above in the limit $1/(\lambda_2 \delta_2) \rightarrow 0$ conforms to that obtained by Ohshima, whose theory disregards the presence of finite flow within the PEM, despite the intrinsic soft nature of polymeric films.

Overall, the dependence of the PZSC on the key quantities $\lambda_2 \delta_2$ and $\kappa \delta_2$ (Figure 3A) is the direct illustration of the electrolyte concentration and hydrodynamic softness dependence of the spatial zone of the film that is electrokinetically active under lateral flow conditions. Roughly speaking, for $\lambda_2 \delta_2 \approx 1$ or lower, which corresponds to permeability values for systems of practical interest,²³ $I_{\text{str}}/\Delta P$ and PZSC increasingly

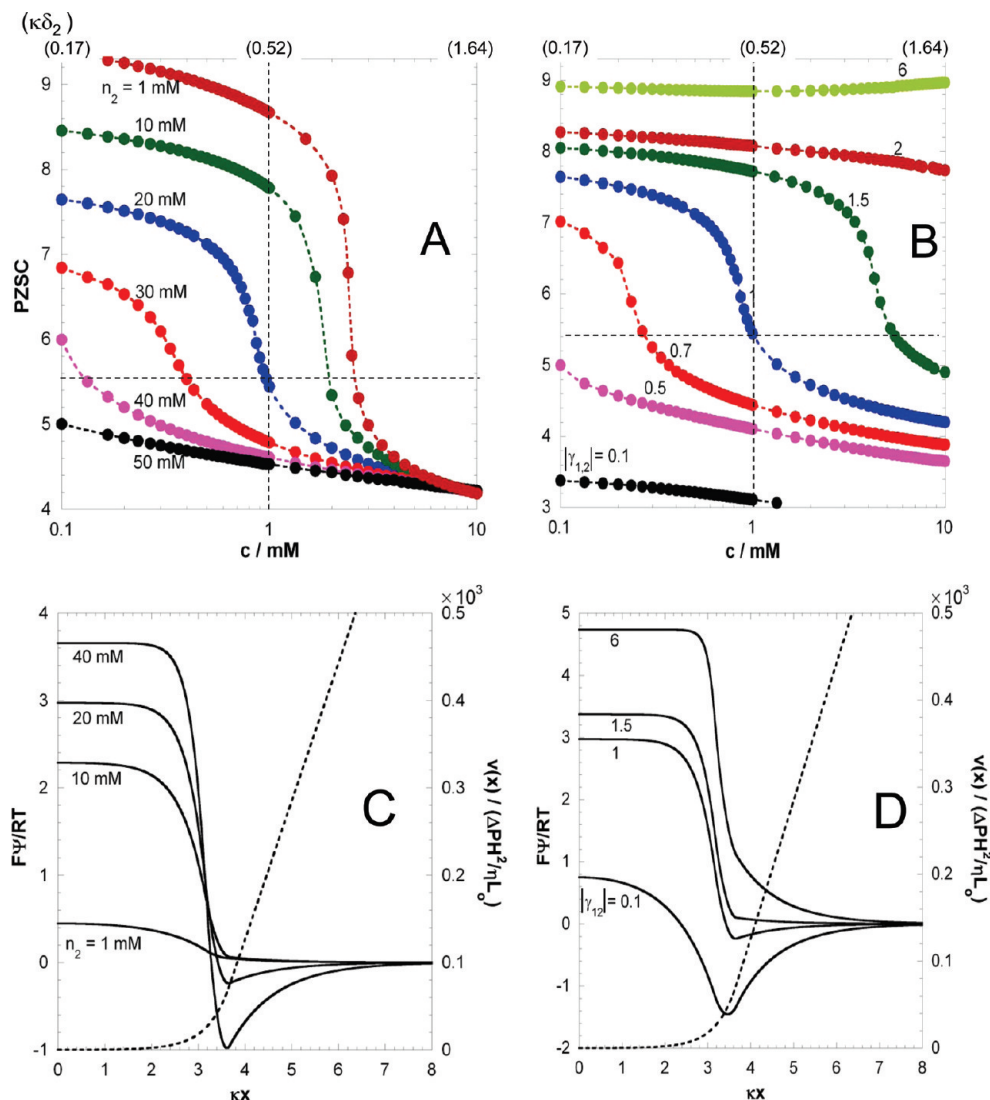


Figure 5. Point of zero streaming current (PZSC) versus electrolyte concentration for various values of (A) site concentration n_2 within layer 2 and (B) ratio $\gamma_{1,2} = \rho_1/\rho_2$ (<0). Other model parameters as in Figure 2. Dotted lines are guides to the eye. (C,D) Dimensionless electrostatic potential (solid lines) and velocity field (dotted lines) across the bilayer film at $pH = 5.45$ and $c = 1$ mM for various values of (C) n_2 and (D) $\gamma_{1,2}$. Other model parameters as in Figure 2. Horizontal and vertical dotted lines in panels A and B indicate pH values and electrolyte concentrations at which potential and velocity field distributions are given in panels C and D, respectively (see text for details).

reflect the electrostatic features of the most internal part of the film with decreasing electrolyte concentration. This shift of the PZSC with c is observed provided that the polymeric film is chemically stratified, that is, there is an inhomogeneous distribution of the protolytic properties of the ionogenic sites from the film carrier surface to the very interface formed between the film and the outer medium solution. This important element is illustrated in the Supporting Information (Figure S1), where we report the dependence of $I_{str}/\Delta P$ on pH, electrolyte concentration c , and hydrodynamic softness λ for a film of thickness δ where positive and negative charges ($\varepsilon_1 = +1/pK_{a,1} = 9$ and $\varepsilon_2 = -1/pK_{a,2} = 4$, respectively) are homogeneously distributed. For such a system, the PZSC does not depend on c or λ , but instead is simply given by the classical expression $PZSC = (pK_{a,1} + pK_{a,2})/2$.

For the sake of simplicity, in the situations discussed above, we considered that the hydrodynamic softness pertaining to the internal layer of the film ($j = 1$) was similar to that of the external

layer ($j = 2$) facing the outer solution medium [i.e., $\omega_{1,2} = k_1/k_2 = (\lambda_1/\lambda_2)^2 = 1$]. In practice, however, the conformation and density of polymer chains within the various layers constituting the film can differ so that the quantities $\omega_{j \in [1, \dots, N-1], N}$ in eq 8 possibly deviate from unity. We report in Figure 3B the dependence of the PZSC on electrolyte concentration at fixed $1/\lambda_2 = 4.5$ nm for various values of $\omega_{1,2}$ from 0 to infinity, which corresponds to the limiting cases where internal layer 1 is free-draining and impermeable to flow, respectively. The results are essentially analogous to those extensively discussed with respect to the data shown in Figure 3A when examining the impact of $1/(\lambda_2\delta_2)$ on the electrolyte concentration dependence of the PZSC. The reasons for this analogy originate from the similar modulations of the velocity distribution across the film when varying $\omega_{1,2}$ at fixed $1/(\lambda_2\delta_2)$ [Figure S2 (Supporting Information) and Figure 3B] or when varying $1/(\lambda_2\delta_2)$ at constant $\omega_{1,2}$ (Figures 4B and 3B). In detail, the electrokinetically active region of the film gradually expands toward layer 1 upon gradual

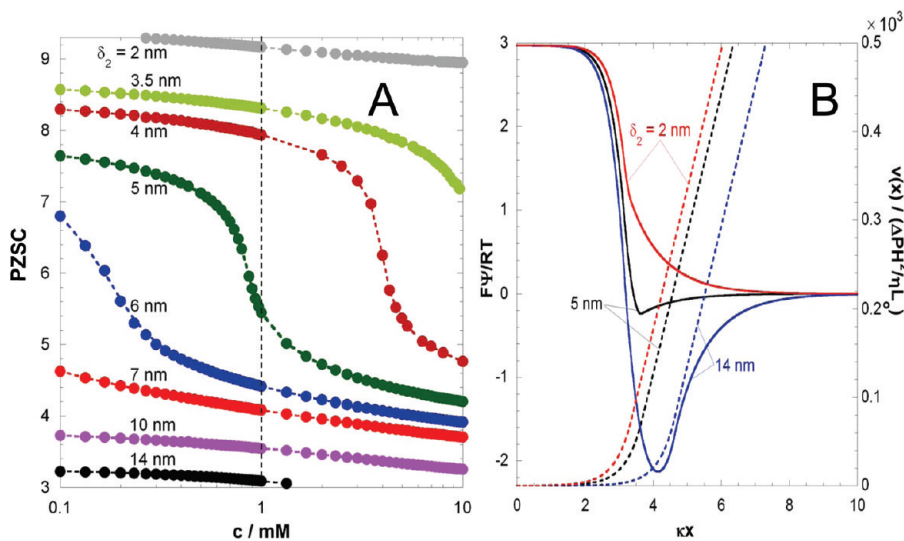


Figure 6. (A) Point of zero streaming current (PZSC) versus electrolyte concentration for various values of the thickness of layer 2 (δ_2). Other model parameters as in Figure 2. Dotted lines are guides to the eye. (B) Dimensionless electrostatic potential (solid lines) and velocity field (dotted lines) across the bilayer film at $\text{pH} = 5.45$ and $c = 1 \text{ mM}$ for various values of δ_2 . Other model parameters as in Figure 2. The vertical dotted line in panel A indicates the electrolyte concentration for which the potential and velocity field distributions are given in panel B (see text for details).

decrease of $\omega_{1,2}$ and/or increase of $1/(\lambda_2 \delta_2)$ following a decrease therein of the friction exerted on the flow.

3.3. Dependence of the Point of Zero Streaming Current (PZSC) on Electrostatic Film Properties and on the Ratio δ_2/δ_1 . In Figure 5A, we report the dependence of the PZSC on the electrolyte concentration for various values of n_2 , the density of ionizable sites carried by layer 2, the other model parameters being those defined earlier for our bilayer assembly of cationic and anionic layers. Although the sigmoid-like decrease of the PZSC with increasing c at fixed n_2 is in line with results previously discussed for $1/(\lambda_2 \delta_2) \approx 1$ (Figure 3A), we observe that (i) for $\kappa \delta_2 \gg 1$, reached at sufficiently high electrolyte concentration, the PZSC becomes independent of n_2 ; (ii) the magnitude of the overall decrease in PZSC as c increases from 0.1 to 10 mM is strongly reduced with increasing n_2 ; (iii) the sigmoid-like decrease of the PZSC with increasing c is steepest for low n_2 ; and (iv) the electrolyte concentration where the rate of decrease of the PZSC with increasing c reaches a maximum is shifted to larger value with decreasing n_2 . Feature i is the result of a significant screening of film charge at extreme values of c or $\kappa \delta_2$, regardless the magnitude of n_2 . The understanding of observations ii–iv requires analysis of the impact of n_2 on the potential distribution across the film. The results are given in Figure 5C for $c = 1 \text{ mM}$, $1/(\lambda_2 \delta_2) = 0.9$, and $\text{pH} \approx 5.45$, which corresponds to the PZSC met under the condition $n_2 = 20 \text{ mM}$ (see Figure 5A). As n_2 increases from 1 to 40 mM, the potential $y(x)$ gradually increases in cationic layer 1, as expected. The bulk potential within layer 1 reaches the Donnan potential in line with $\kappa \delta_1 \approx 3$ under the conditions of Figure 5C. The striking result is that the potential within the negatively charged layer 2 becomes negative only for $n_2 > 10 \text{ mM}$ and remains positive for lower n_2 . This is explained by the conjunction of two factors. First, the electric double layer does not extend significantly within the outermost layer of the film ($\kappa \delta_1 \approx 0.5$), and second, the electric field at the interface between layers 1 and 2 must exceed a threshold value (not reached for $n_2 < 10 \text{ mM}$) for the potential to reverse the sign across the film. In line with the analysis of potential/charge regulation processes governing

heterointeraction of hard interfaces,³¹ one can speak of “strong” and “weak” double layers when referring to layers 1 and 2, respectively, for $n_2 < 10 \text{ mM}$. With the potential distributions of Figure 5C in mind, the dependence of the PZSC on n_2 , as depicted in Figure 5A, is explained as follows: We start from the PZSC situation reached under the conditions $n_2 = 20 \text{ mM}$ and $c = 1 \text{ mM}$. With decreasing n_2 at fixed c , the weak character of the electric double layer span within layer 2 gradually hinders sign reversal of the potential across the film (Figure 5C) so that, in turn, I_{str} becomes positive. To recover the PZSC condition, it is necessary to increase the solution pH so as to increase the number density of negatively charged sites within layer 2, in agreement with results of Figure 5A (see vertical dotted line therein). Conversely, with increasing n_2 above 20 mM at fixed c , the potential within layer 2 becomes more negative, as does I_{str} , because the flow mostly probes charges located within the outer region of the film, as evidenced by the velocity profile given in Figure 5C for $1/(\lambda_2 \delta_2) = 0.9$. To re-establish the conditions defining the PZSC, it is necessary to diminish the dissociation of sites located in layer 2, which is achieved by decreasing the pH, in line with Figure 5A. Finally, as mentioned earlier, the steepest part of the sigmoid-like decrease in PZSC with increasing electrolyte concentration is shifted to greater c with decreasing n_2 . To explain this behavior, we reason at fixed pH ≈ 5.45 and start from the situation $n_2 = 20 \text{ mM}$ and $c = 1 \text{ mM}$ (see horizontal dotted line in Figure 5A). Upon decrease of n_2 , the electrostatic potential becomes positive within layer 2 and all across the film (Figure 5C), so that $I_{\text{str}} > 0$. To return to conditions where $I_{\text{str}} = 0$, the potential must recover a negative sign at the outermost region of the film. To achieve this, it is necessary to increase the electrolyte concentration. Indeed, doing so, one increases $\kappa \delta_2$ and therefore allows the electric double layer to fully develop within layer 2 where the electric potential is able to reach the negative Donnan value (not shown). This increase in $\kappa \delta_2$ to retrieve the PZSC condition when increasing n_2 at fixed pH is in accordance with the results of Figure 5A.

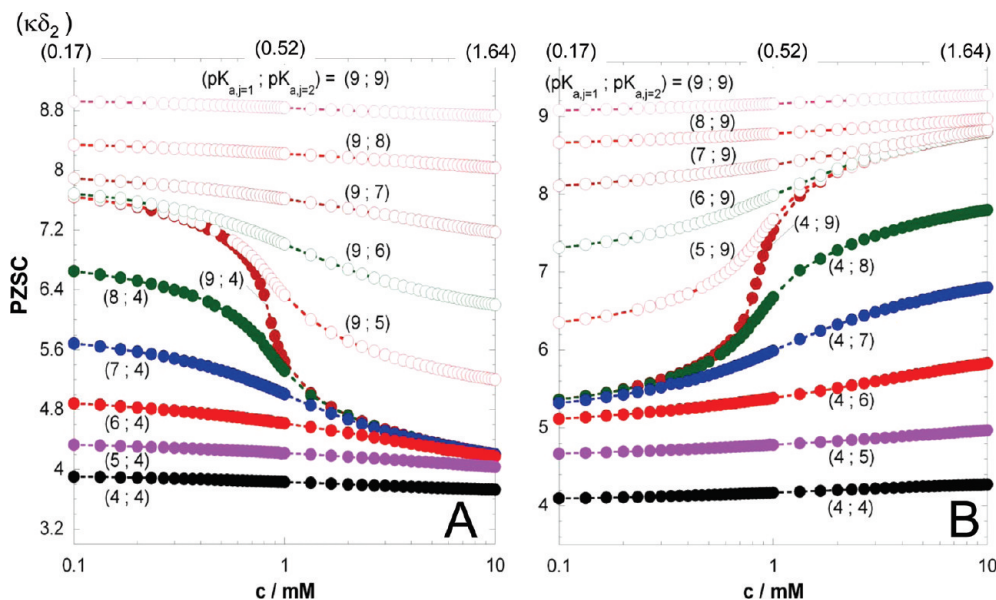


Figure 7. Point of zero streaming current (PZSC) versus electrolyte concentration for various sets of $(pK_{a,j=1}; pK_{a,j=2})$ values. Other model parameters as in Figure 2, except (A) $\varepsilon_1 = +1$, $\varepsilon_2 = -1$ and (B) $\varepsilon_1 = -1$, $\varepsilon_2 = +1$. Dotted lines are guides to the eye.

In Figure 5B, we give the dependence of the PZSC on c for a fixed $\rho_2/F = -20$ mM and various values of the ratio $\gamma_{1,2} = \rho_1/\rho_2 (<0)$. At high $\kappa\delta_2$, where modulation in $\gamma_{1,2}$ least affects the potential distribution across layer 2, the trends depicted in Figure 5B are analogous to those discussed at high concentrations in Figure 3B, where the dependence of the PZSC on $\omega_{1,2} = k_1/k_2$ was examined. Within this concentration regime, increasing $\gamma_{1,2}$ (or decreasing $\omega_{1,2}$) at fixed c results in a stronger role played by the inner layer 1 in determining I_{str} because the number of charges located therein is larger (or the friction it exerts on the flow is lower). At lower electrolyte concentration (i.e., lower $\kappa\delta_2$), varying $\gamma_{1,2}$ significantly changes the potential profile within layer 2 (Figure 5D). In detail, increasing $\gamma_{1,2}$ leads to a stronger electric double layer in layer 1, which prevents, for sufficiently large values of $\gamma_{1,2}$, the potential from changing sign across the film. Qualitatively, this dependence of the potential sign across the film on $\gamma_{1,2}$ is analogous to that resulting from a decrease of n_2 as discussed in Figure 5C. In turn, the dependence of the PZSC with increasing $\gamma_{1,2}$ at low $\kappa\delta_2$ (Figure 5B) is similar to that displayed in Figure 5A with decreasing n_2 at low concentration.

The impact of the ratio δ_2/δ_1 on the concentration dependence of the PZSC is now briefly discussed on the basis of the simulations displayed in Figure 6A. When comparing that figure with Figure 5B, we note that decreasing δ_2/δ_1 or increasing $\gamma_{1,2}$ qualitatively leads to a similar dependence of the PZSC on c . The reason for the similarity is that the corresponding variations in electrostatic potential distribution essentially display the same features, in particular with regard to conditions underlying the presence/absence of sign reversal for the potential across the film (Figures 5D and 6B). Finally, for the sake of completeness, Figure 7 demonstrates that the greater the difference $|pK_{a,1} - pK_{a,2}|$, the greater the magnitude of the shift in PZSC with increasing electrolyte concentration, as intuitively anticipated. In addition, the direction of the shift of the PZSC with increasing c is determined by the sign of the difference $(pK_{a,1} - pK_{a,2})$ (Figure 7B). The latter result is

important because straightforward examination of the PZSC measured as a function of electrolyte concentration can provide information on the signs of the charges that are directly facing the solution side of the interface and of those embedded deeper within the film under given pH conditions. Such information is necessarily required for the understanding of the electrostatic interaction of the film with neighboring charged colloids.²⁶

3.4. Dependence of the PZSC on the Diffuseness of the Soft Multilayered Film. In the preceding examples, the basic electrokinetic properties of PEMs were discussed for the simplest situation of a bilayer film made from the assembly of a cationic layer and an anionic layer whose density distributions of ionizable sites follow step-function-like profiles, that is, $\alpha_{j=1,2} \rightarrow 0$ in eqs 3 and 4. In practice, heterogeneous swelling of the film and interactions between layers 1 and 2 can lead to position-dependent distributions of the density of polymer segments or, equivalently, of the density of ionizable sites $n(x)$ and friction coefficient $k(x)$.^{19,20,23–25} Figure 8 clarifies the impact of the diffuseness of the anionic layer 2 ($\alpha_1 \rightarrow 0$, $\alpha_2 > 0$) on the PZSC for the bilayer film. Before discussing Figure 8, it should be realized that interphasic diffuseness impacts both electrostatic and hydrodynamic profiles across soft interphases along the lines extensively detailed in previous experimental and theoretical works for monolayered polymeric systems.^{19,20,22,23} This multiparametric influence makes it difficult to generalize the effects of α_j on the PZSC. Under conditions of Figure 8, increasing α_2 at fixed c leads to a decrease of the PZSC. This effect, similar to that discussed in Figure 6A, is due to the gradual extension of layer 2 (inset Figure 8) whose contribution in governing I_{str} and PZSC then becomes increasingly important. As a result, to retrieve the conditions where $I_{str} = 0$, the solution pH must be decreased to decrease the magnitude of the overall charge carried by layer 2 and, therewith, to re-establish the appropriate balance between positive and negative charges across the electrokinetically active zone of the bilayer. The concentration where the decrease of the PZSC with increasing c is steepest is shifted to lower values with increasing α_2 , in line with the trend depicted in Figure 6A.

Increasing α_2 effectively results in an extension of layer 2, and the underlying modulation of the PZSC is qualitatively similar to that depicted in Figure 6A for homogeneous layers with increasing δ_2 . In addition, the impact of α_2 on the PZSC is most pronounced at low c . In this regime of concentration where $\kappa\alpha_2 \leq 1$, the electric double layer significantly covers regions of the diffuse film with a spatially dependent distribution of the polymer segment density. In turn, I_{str} and PZSC are most affected by α_2 at low c . Finally, for sufficiently large α_2/δ_2 , the dependence of the PZSC on the electrolyte concentration is weakest. This configuration corresponds to strong heterogeneous expansion of layer 2 in bulk solution, and the corresponding effect on the PZSC is then analogous to that discussed with respect to Figure 6A at large values of δ_2/δ_1 .

For the sake of conciseness, the ways in which concomitant modulations of α_2 and α_1 affect the electrokinetics and PZSC of the bilayer film are not discussed here. As for monolayered systems,^{19,20,22,23,32} such an analysis requires careful evaluation of the impact of interphasial diffuseness on both potential and velocity field profiles across the electrokinetically active part of the film.

4. ILLUSTRATIONS

In this section, the basics of the theory given in sections 2 and 3 are illustrated with streaming current data collected as a function of pH and electrolyte concentration for two chemically stratified thin films: a poly(ethylene imine) (PEI)/poly(acrylic acid) (PAA) bilayer (hereafter denoted as system 1) and an artificial bilayer lipid membrane (BLM) supported by a PEI cushion (system 2). The experimental protocols and procedural details for the preparation of these two systems are given first (section 4.1), and their electrokinetic properties are discussed on the basis of the theory (section 4.2).

4.1. Experimental Section. *Poly(ethylene imine) Films.* Poly(ethylene imine) (500000 g/mol, BASF SE, Ludwigshafen, Germany) was covalently attached to Teflon AF surfaces using a low-pressure plasma treatment. The Teflon AF films were prepared by spin-coating onto hydrophobized silicon carriers as described in detail elsewhere.³³ The Teflon AF surface was hydrophilized by an argon plasma treatment,³³ allowing the spin coating of a poly(ethylene imine) solution (7.5 mg/mL in methanol). Subsequently, the polymer was immobilized by a second argon plasma treatment,³³ enabling the covalent attachment of the polymer to the surface as well as internal cross-linking. After the sample had been rinsed with methanol, the dry film thickness of the PEI layer was measured by ellipsometry (M-44, J. A. Woolam Co. Inc., Lincoln, NE) and found to be about 10 nm.

Poly(acrylic acid)/Poly(ethylene imine) Bilayers. Poly(acrylic acid) (450000 g/mol, St. Louis, MO) was adsorbed onto PEI-coated sample carriers (see above) by injecting a 0.1 mM aqueous PAA solution (related to the number of charged repeat units of the polymer, solution pH = 4.2) into the measuring cell. After 5 min of incubation, the cell was extensively rinsed with deionized water. In situ ellipsometry studies revealed a PAA film thickness (swollen layer) of ~5 nm. The polyelectrolyte bilayer was equilibrated in 0.1 and 10 mM KCl solution by systematically changing the solution pH in the range used for the electrokinetic measurements (two cycles from high to low pH).

Polymer-Cushioned Bilayer Lipid Membranes. Supported bilayer lipid membranes were prepared from the phospholipid

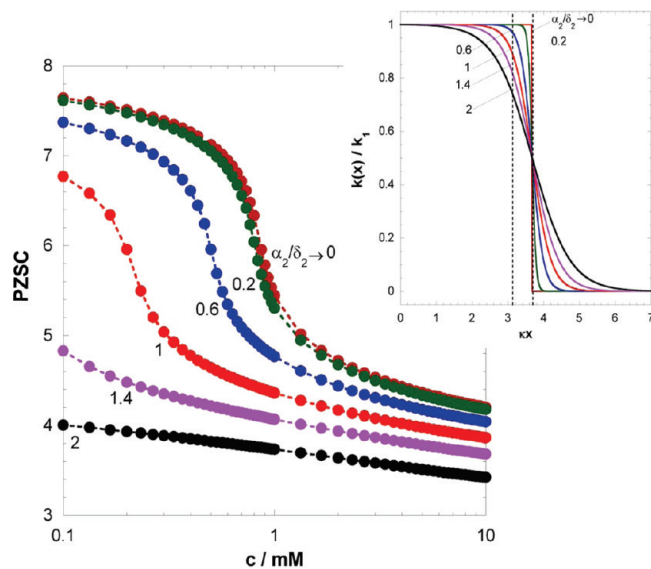


Figure 8. Point of zero streaming current (PZSC) versus electrolyte concentration for various values of α_2/δ_2 (indicated). Inset: Corresponding spatial profiles of the normalized friction coefficient $k(x)/k_1$. Other model parameters as in Figure 2. Dotted lines are guides to the eye.

1,2-dioleoyl-sn-glycero-3-phospho-(1'-rac-glycerol) (DOPG, Avanti Polar Lipids, Alabaster, AL) onto PEI cushions (see above) as described in detail elsewhere.³⁴ In short, lipid vesicles containing DOPG were prepared by mixing the dried lipid in chloroform, evaporating the solvent with argon gas and additionally under vacuum for 4 h so as to completely remove the solvent, and hydrating in pH 4 saline (10 mM NaCl, 5 mM CaCl₂, adjusted to pH 4 with 0.1 M HCl). The mixture was extruded (Mini Extruder, Avanti Polar Lipids, Alabaster, AL) at least 31 times through 50-nm-diameter pores in a polycarbonate membrane (Whatman Ltd., Kent, U.K.) following the procedure of Hope et al.³⁴ Subsequently, the measuring cell was assembled, and a lipid vesicle solution (0.2 mg/mL in KCl solution) was injected into the cell. The surfaces were incubated at 22 °C for 2 h. After incubation, the cells were excessively rinsed at least 10 times with KCl solution.

Electrolyte Solutions. The electrolyte solutions used in this study (0.1–10 mM KCl, pH 2.5–10) were prepared from vacuum-degassed deionized water (Milli-Q gradient A10, Millipore Co., Billerica, MA) by addition and/or appropriate dilution of 0.1 M KCl, HCl, and KOH stock solutions (VWR International GmbH, Darmstadt, Germany).

Electrokinetic Measurements. Streaming current (I_{str}) measurements were performed at rectangular streaming channels (20 mm × 10 mm × 30 μm) formed by two sample surfaces using the Microslit Electrokinetic Setup.³⁵ The electrokinetic measurements were started at alkaline pH. For each pH value and electrolyte concentration tested in this study, systems were equilibrated for about 40 min prior to measurement. The respective concentrations of all ions present in the medium were back-computed by appropriately taking into account dilution factors and contributions stemming from the addition of aliquots of 0.1 M HCl and KOH solutions used to fix the solution pH.

4.2. Electrokinetic Results, Discussion. The pressure-normalized streaming currents, $I_{\text{str}}/\Delta P$, measured for systems 1 and 2

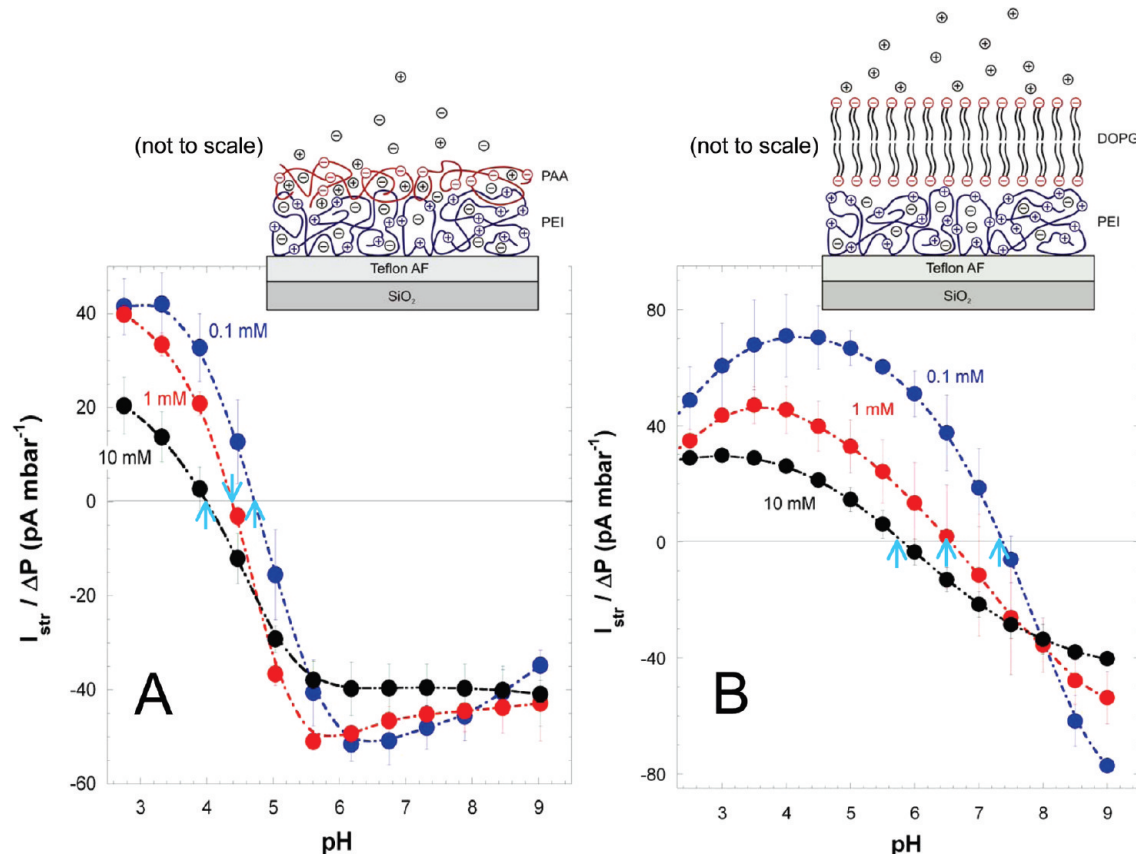


Figure 9. Ratio between streaming current (I_{str}) and applied pressure (ΔP) as a function of pH as measured at three electrolyte concentrations (indicated) for (A) PEI/PAA and (B) PEI/lipid bilayer membrane. Schematic representations (not to scale) of the soft multilayered interphases considered are given in the insets. For both systems, the arrows underline the expected decrease of the PZSC with increasing electrolyte concentration. Dotted lines are guides to the eye.

as functions of pH (2.5–9) and electrolyte concentration (0.1–10 mM KCl) are reported in parts A and B, respectively, of Figure 9, where schematic representations of the systems considered are also displayed. We provide below a qualitative discussion of the electrokinetic data with the support of the theoretical framework detailed in sections 2 and 3.

System 1 (PEI/PAA Bilayer). The positive charge located within the internal PEI component of the PEI/PAA bilayer film originates from the protonation of primary, secondary, and tertiary amines with associated pK values of ~ 8.6 –9.50, 10.9, and 7.1–8.50, respectively (where the values were recently derived by analyzing streaming current and surface conductivity data of a PEI monolayer;³² see Figure S3, Supporting Information). The negative charge of the PAA component stems from the deprotonation of carboxylic groups with a pK value of ~ 3.3 –4 (Figure S3, Supporting Information).³² The respective magnitudes of these ionization constants are consistent with the observed decrease of the PZSC for the PEI/PAA system with increasing electrolyte concentration (Figure 9A), as expected from theory (Figure 7A). According to our formalism, the presence of such concentration dependence of the PZSC implies that the potential distribution within the peripheral PAA layer must be significantly affected by the charge carried by the internal PEI layer. This is indeed the case because the thickness of that PAA layer, as evaluated from ellipsometry (~ 5 nm in swollen state), is on the order of—or lower than—the Debye layer thickness in the concentration range from 0.1 to 10 mM. In line

with the simulation results of Figure 1 that pertain to a polyanion/polycation bilayer whose characteristics in terms of thickness and pK values are basically comparable to those of the PEI/PAA bilayer, the trends depicted in Figure 9A are intermediate between those extensively analyzed in ref 32 for PEI and PAA layers, taken separately (Figure S3, Supporting Information). In particular, the presence of a maximum in $|I_{\text{str}}/\Delta P|$ at sufficiently high concentrations and $\text{pH} > 5$ (Figure 9A) is reminiscent of that obtained for thicker PAA films.³² That maximum, whose presence is due to heterogeneous extension of PAA chains following swelling, gradually disappears with increasing electrolyte concentration, as extensively discussed for PAA monolayers.³²

Regarding system 1, appropriate quantitative analysis of electrokinetic data requires knowledge on the distribution of polymer chains across the film, in particular, in the interphasic region marking the transition between layer 1 (PEI) and layer 2 (PAA). This distribution depends on pH and solution ionic strength (swelling/shrinking processes, interdiffusion PEI/PAA) and dramatically impacts the electrokinetics, as evidenced in previous work for soft monolayered thin-films^{22,23,32} and briefly discussed in this article for multilayered systems (Figure 8). Contrary to the case of monolayered films,^{22,23,32} such information on the pH and ionic strength dependence of the multilayered film structure cannot be easily obtained with the help, for example, of independent surface conductivity and ellipsometry measurements. Instead, spatially resolved data all across the

bilayer film structure are required and can be obtained by, for example, refined neutron or X-ray reflectivity measurements.³⁶ Such analysis is beyond the scope of the current work, which aims to establish the basic electrokinetic properties of multilayered films and their relation to the necessarily complex electrostatic and permeability features of the various constituent layers.

System 2 (PEI-Cushioned DOPG Membrane). DOPG is a phospholipid that bears a negative charge at intermediate and alkaline pH as a result of the ionization of phosphate groups. The spatial separation between the charge carried by the outer and inner leaflets of the bilayer lipid membrane (Figure 9B) is about 4 nm,³⁷ that is, lower than or on the order of the Debye length for ionic strengths in the range of 0.1–10 mM. Accordingly, the PEI-cushioned DOPG membrane fulfills the conditions for a shift of the PZSC with increasing electrolyte concentration, in line with the respective pH dependence of the charges located within the inner and outer components of the system. This trend is indeed observed, as the PZSC decreases from 7.4 to 5.8 in the range from 0.1 to 10 mM. In addition, contrary to system 1, the curves $I_{\text{str}}/\Delta P$ versus pH obtained for system 2 at 0.1, 1, and 10 mM KCl exhibit a common intersection point (at $\text{pH} \approx 8$). This feature is expected for multilayered films provided that the thickness of the constituting layers remains independent of pH and electrolyte concentration (Figure 2). Any modulation of the layer thicknesses as a result of pH- and/or concentration-dependent structural variation, for example, would necessarily induce a modification of the respective contributions of the various layers in determining the overall electrokinetic response of the system and, in turn, would lead to the absence of a common intersection point for the $I_{\text{str}}/\Delta P$ versus pH curves measured at various c values. In the case of a PEI-cushioned DOPG membrane, the conditions required for the presence of this common intersection point are well-satisfied, as the PEI layer thickness and structure barely depend on pH and electrolyte concentration³² and the thickness of bilayer lipid membranes varies only marginally with changing solution pH and salinity. Quantitative reconstruction of the data displayed in Figure 9B with the theory of section 2 would require modeling of the spatial distribution of dielectric permittivity across the film, as well as knowledge of the structure and local charge compensation at the boundary between the polymer cushion and the inner leaflet of the membrane. Because of the versatile application of supported bilayer lipid membranes as models for natural cell membranes, this analysis will be performed in a further study with the help of spatially resolved data acquired by X-ray reflectivity.

5. CONCLUSIONS

In this article, we report a formalism for comprehending the electrokinetic properties of soft multilayered films. The respective contributions of the constitutive layers in determining the streaming current of the film as a whole are thoroughly discussed. In particular, it is demonstrated that the point of zero streaming current (PZSC) generally depends on the electrolyte concentration (neutral background electrolyte) and is further strongly determined by the respective thickness, hydrodynamic softness, structure (diffuseness), density, and protolytic properties of functional groups in the various layers constituting the film. The basics of the theory are supported by electrokinetic measurements performed on two different chemically stratified thin films, a PEI/PAA PEM and a PEI/lipid bilayer membrane. Straightforward extension of the theory

would include, for example, the account of dielectric permittivity gradient across the multilayered film, which might be of practical interest for systems consisting of polyelectrolyte layers that differ significantly in hydrophilic/hydrophobic balance. In addition, accounting for chain elasticity in the various layers composing the film could help in explaining their potential overlap and the formation of inner film regions where layer charges are mutually screened.

The theoretical framework detailed in this report offers a solid basis for understanding the electrokinetics of complex soft interphases beyond the conventional Smoluchowski equation that is inapplicable for soft monolayered and multilayered polymeric systems. In addition, the theory highlights that the PZSC for soft chemically stratified films is not the pH value where the overall film charge is zero (the so-called isoelectric point, IEP). Instead, the PZSC necessarily reflects richer information on the respective hydrodynamic, electrostatic, and structural properties of the various layers forming the PEM. Such information is required for understanding, for example, the sorption properties of PEMs and their propensity to act as reservoirs for charged (nano)colloids or biomacromolecules (proteins) within the framework of biomedical applications.

■ ASSOCIATED CONTENT

S Supporting Information. Semianalytical derivation of the streaming current for soft multilayered films within the Debye–Hückel approximation in the limits $\alpha_{j=1,\dots,N} \rightarrow 0$ (i.e., layers constituting the films are homogeneous) (sections I–III). Ratio $I_{\text{str}}/\Delta P$ versus pH for various electrolyte concentrations and hydrodynamic softness in the situation where the positive and negative charges of the bilayer film of Figure 2 are uniformly distributed (Figure S1). Distribution of the dimensionless velocity field across the bilayer film of Figure 3B for various values of $\omega_{1,2}$ (Figure S2). Ratio $I_{\text{str}}/\Delta P$ as a function of pH and ionic strength for PEI and PAA monolayers, using data extracted from ref 32 (Figure S3). This information is available free of charge via the Internet at <http://pubs.acs.org/>.

■ AUTHOR INFORMATION

Corresponding Author

*E-mail: jerome.duval@ensg.inpl-nancy.fr. Tel: 00 33 3 83 59 62 63. Fax: 00 33 3 83 59 62 55.

■ ACKNOWLEDGMENT

The authors thank Katrin Taetz and Nelly Rein (Leibniz Institute of Polymer Research Dresden) for the preparation of PEI/PAA films, as well as for performing the electrokinetic measurements. J.F.L.D. acknowledges the French program ANR-07-JCJC-0024-01 PHYSCHEMBACT and the European Union's Seventh Framework Program FP7/2007-2013 (Grant 244405, BIOMONAR project) for financing this research.

■ REFERENCES

- (1) Decher, G.; Hong, J. D.; Schmitt, J. *Thin Solid Films* **1992**, *210/211*, 831–835.
- (2) Schönhoff, M. *J. Phys.: Condens. Matter* **2003**, *15*, R1781–R1808.
- (3) Schönhoff, M. *Curr. Opin. Colloid Interface Sci.* **2003**, *8*, 86–95.
- (4) Von Klitzing, R.; Wong, J. E.; Jaeger, W.; Steitz, R. *Curr. Opin. Colloid Interface Sci.* **2004**, *9*, 158–162.

- (5) Glinel, K.; Dejugnat, C.; Prevot, M.; Schöler, B.; Schönhoff, M.; Von Klitzing, R. *Colloids Surf. A* **2007**, *303*, 3–13.
- (6) Jaber, J. A.; Schlenoff, J. B. *Curr. Opin. Colloid Interface Sci.* **2006**, *11*, 324–329.
- (7) Schlenoff, J. B. *Langmuir* **2009**, *25*, 14007–14010.
- (8) Caruso, F.; Trau, D.; Möhwald, H.; Renneberg, R. *Langmuir* **2000**, *16*, 1485–1488.
- (9) Licherter, J. A.; Van Vliet, K. J.; Rubner, M. F. *Macromolecules* **2009**, *42*, 8573–8586.
- (10) Hoffmann, K.; El-Hashani, A.; Tieke, B. *Macromol. Symp.* **2010**, *287*, 22–31.
- (11) Müller, M.; Kessler, B.; Houbenov, N. *Biomacromolecules* **2006**, *7*, 1285–1294.
- (12) Mijares, G. I.; Reyes, D. R.; Geist, J.; Gaitan, M. J. *Res. Natl. Inst. Stand. Technol.* **2010**, *115*, 61–73.
- (13) Wong, J. E.; Richtering, W. *Curr. Opin. Colloid Interface Sci.* **2008**, *13*, 403–412.
- (14) Delgado, A. V.; González-Caballero, F.; Hunter, R. J.; Koopal, L. K.; Lyklema, J. J. *Colloid Interface Sci.* **2007**, *309*, 194–224.
- (15) Dukhin, S. S.; Semenikkin, N. M.; Bychko, W. A. In *Surface Forces in Thin Layers*; Derjaguin, B. V., Ed.; Acad. Science USSR, Nauka: Moscow, USSR, 1979; pp 85–93 (in Russian).
- (16) Ohshima, H.; Kondo, T. J. *Colloid Interface Sci.* **1990**, *135*, 443–448.
- (17) Shinagawa, T.; Ohshima, H.; Kondo, T. *Biophys. Chem.* **1992**, *43*, 149–156.
- (18) Dukhin, S. S.; Zimmermann, R.; Werner, C. *J. Colloid Interface Sci.* **2004**, *274*, 309–318.
- (19) Duval, J. F. L.; van Leeuwen, H. P. *Langmuir* **2004**, *20*, 10324–10336.
- (20) Duval, J. F. L. *Langmuir* **2005**, *21*, 3247–3258.
- (21) Dukhin, S. S.; Zimmermann, R.; Werner, C. *J. Colloid Interface Sci.* **2008**, *328*, 186–195.
- (22) Duval, J. F. L.; Zimmermann, R.; Cordeiro, A. L.; Rein, N.; Werner, C. *Langmuir* **2009**, *25*, 10691–10703.
- (23) Zimmermann, R.; Kuckling, D.; Kaufmann, M.; Werner, C.; Duval, J. F. L. *Langmuir* **2010**, *26* (23), 18169–18181.
- (24) Dukhin, S. S.; Zimmermann, R.; Duval, J. F. L.; Werner, C. *J. Colloid Interface Sci.* **2010**, *350*, 1–4.
- (25) Yezek, L.; Duval, J. F. L.; van Leeuwen, H. P. *Langmuir* **2005**, *21*, 6220–6227.
- (26) Duval, J. F. L.; Merlin, J.; Anantha, P. *Phys. Chem. Chem. Phys.* **2011**, *13*, 1037–1053.
- (27) Langlet, J.; Gaboriaud, F.; Gantzer, C.; Duval, J. F. L. *Biophys. J.* **2008**, *94*, 3293–3312.
- (28) Donath, E. D.; Walther, D.; Shilov, V. N.; Knippel, E.; Budde, A.; Lowack, K.; Helm, C. A.; Möhwald, H. *Langmuir* **1997**, *13*, 5294–5305.
- (29) Ohshima, H. *Adv. Colloid Interface Sci.* **1995**, *62*, 189–235.
- (30) Duval, J. F. L.; Ohshima, H. *Langmuir* **2006**, *22*, 3533–3546.
- (31) Lyklema, J.; Duval, J. F. L. *Adv. Colloid Interface Sci.* **2005**, *114*, 27–45.
- (32) Duval, J. F. L.; Küttner, D.; Nitschke, M.; Werner, C.; Zimmermann, R. Interrelations between charging, structure and electrokinetics of nanometric polyelectrolyte films. *J. Colloid Interface Sci.*, published online July 7, 2011, <http://dx.doi.org/10.1016/j.jcis.2011.06.063>.
- (33) Cordeiro, A. L.; Zimmermann, R.; Gramm, S.; Nitschke, M.; Janke, A.; Schäfer, N.; Grundke, K.; Werner, C. *Soft Matter* **2009**, *5*, 1367–1377.
- (34) Hope, M. J.; Bally, M. B.; Webb, G.; Cullis, P. R. *Biochim. Biophys. Acta* **1985**, *812*, 55–65.
- (35) Werner, C.; Körber, H.; Zimmermann, R.; Dukhin, S. S.; Jacobasch, H.-J. *J. Colloid Interface Sci.* **1998**, *208*, 329–346.
- (36) Daillant, J.; Guibaut, A., Eds. *X-ray and Neutron Reflectivity: Principles and Applications*; Springer: Heidelberg, Germany, 1999.
- (37) Vacha, R.; Jurkiewicz, P.; Petrov, M.; Berkowitz; Böckmann, R. A.; Barucha-Kraszewska, J.; Hof, M.; Jungwirth, P. *J. Phys. Chem. B* **2010**, *114*, 9504–9509.

SUPPORTING INFORMATION

Electrohydrodynamics of Soft Polyelectrolyte Multilayers: Point of Zero-Streaming Current.

Jérôme F. L. Duval,^{1*} David Küttner,² Carsten Werner,^{2,3} Ralf Zimmermann²

¹ Laboratoire Environnement et Minéralurgie, Nancy-Université, CNRS UMR 7569, 15 avenue du Charmois, B.P. 40, 54501 Vandoeuvre-lès-Nancy, cedex France.

² Leibniz Institute of Polymer Research Dresden, Max Bergmann Center of Biomaterials Dresden, Hohe Strasse 6, 01069 Dresden, Germany.

³ University of Toronto, Institute of Biomaterials and Biomedical Engineering, 5 King's College Road, Toronto, Ontario, Canada, M5S 3G8.

* Corresponding author:

Jérôme F. L. Duval: jerome.duval@ensg.inpl-nancy.fr
Tel: 00 33 3 83 59 62 63. Fax: 00 33 3 83 59 62 55.

Summary.

We report here an analytical evaluation of the streaming current, I_{str} , of poorly to moderately charged polyelectrolyte multilayers (PEM) in the limits of a symmetrical $z:z$ electrolyte of concentration c^∞ . Furthermore, we assume that the N layers of the PEM are homogeneously distributed, *i.e.* $\alpha_{j=1,\dots,N} \rightarrow 0$. We first derive an analytical expression for the electrostatic potential distribution across the PEM within the Debye-Hückel approximation, then formulate the spatial profiles for the pressure driven-flow inside and outside the PEM, and finally provide the corresponding analytical equation for I_{str} . If not specified, the meaning of the various symbols used here is that defined in the main text.

I. Electrostatics.

Under conditions of low electrostatic potentials ($y(x) \ll 1$), and homogeneous profile ($\alpha_{j=1,\dots,N} \rightarrow 0$) for the concentration of ionizable groups within each layer of the PEM, the non-linear Poisson Boltzmann equation (eq 9 in the main text) can be linearized and written for a $z:z$ electrolyte in the form

For $X_{j-1} \leq X \leq X_j$ and $j = 1, \dots, N+1$:

$$\frac{d^2 y_j(X)}{dX^2} - (\kappa H)^2 \left[1 + \frac{\tilde{\rho}_j \theta_j \varepsilon_j}{z(1+\theta_j)^2} \right] y_j(X) = -(\kappa H)^2 \frac{\tilde{\rho}_j}{(1+\theta_j)}, \quad (S1)$$

where $X_j = x_j / H$, $y_j(X) = zF\psi(X_{j-1} \leq X \leq X_j) / RT$ is the dimensionless potential distribution across the j th-layer of the PEM, $\tilde{\rho}_j = \rho_{j=1} / (2Fzc^\infty)$ is the dimensionless charge density within layer j and $\theta_j = 10^{-\varepsilon_j(pK_{a,j} - pH)}$. In eq S1, the index $j = N+1$ refers to the electrolyte solution (region outside the PEM without fixed charges), *i.e.* $\tilde{\rho}_{N+1} = 0$. The solutions of eq S1 read as:

For $X_{j-1} \leq X \leq X_j$ and $j = 1, \dots, N$:

$$y_j(X) = A_j \cosh(\bar{\kappa}_j H X) + B_j \sinh(\bar{\kappa}_j H X) + \beta_j \quad (S2)$$

For $X_N \leq X$:

$$y_{N+1}(X) = A_{N+1} \exp(-\bar{\kappa}_{N+1} H X), \quad (S3)$$

where $A_{j=1,\dots,N+1}$ and $B_{1,\dots,N}$ are constants to be determined, $\bar{\kappa}_j = \kappa \left[1 + \frac{\tilde{\rho}_j \theta_j \varepsilon_j}{z(1+\theta_j)^2} \right]^{1/2}$,

$\beta_j = \left(\frac{\kappa}{\bar{\kappa}_j} \right)^2 \frac{\tilde{\rho}_j}{(1+\theta_j)}$. Applying adequately the boundaries for $y(X)$ as specified in the main text together with the required continuity equations for the potential and electric field at the positions $X_{j=1,\dots,N}$, we show that the $A_{j=1,\dots,N+1}$ and $B_{1,\dots,N}$ are solutions of the algebraic equations written in the matrix form

$$T \cdot \vec{S}_{\text{Elec}} = \vec{C}_{\text{Elec}}, \quad (\text{S4})$$

where \vec{S}_{Elec} and \vec{C}_{Elec} are the $2N+1$ column vectors defined by:

$$\vec{S}_{\text{Elec}} = \begin{pmatrix} A_1 \\ A_2 \\ \vdots \\ A_N \\ A_{N+1} \\ B_1 \\ B_2 \\ \vdots \\ B_N \end{pmatrix}, \quad \vec{C}_{\text{Elec}} = \begin{pmatrix} \beta_2 - \beta_1 \\ \beta_3 - \beta_2 \\ \vdots \\ \beta_N - \beta_{N-1} \\ -\beta_N \\ 0 \\ \vdots \\ 0 \end{pmatrix} \quad (\text{S5,S6})$$

and T the $(2N+1) \times (2N+1)$ Jacobian matrix of which elements $t_{i,j}$ are defined by the relationships:

$$i = 1, \dots, N-1 : \quad \begin{cases} t_{i,i} = \cosh(\bar{\kappa}_i H X_i) \\ t_{i,i+N+1} = \sinh(\bar{\kappa}_i H X_i) \\ t_{i,i+1} = -\cosh(\bar{\kappa}_{i+1} H X_i) \\ t_{i,i+N+2} = -\sinh(\bar{\kappa}_{i+1} H X_i) \end{cases} \quad (\text{S7-S10})$$

$$i = N : \quad \begin{cases} t_{i,i} = \cosh(\bar{\kappa}_i H X_i) \\ t_{i,i+N+1} = \sinh(\bar{\kappa}_i H X_i) \\ t_{i,i+1} = -\exp(-\bar{\kappa}_{i+1} H X_i) \end{cases} \quad (\text{S11-S13})$$

$$i = N+1, \dots, 2N-1 : \quad \begin{cases} t_{i,i-N} = (\bar{\kappa}_{i-N} / \bar{\kappa}_{i-N+1}) \sinh(\bar{\kappa}_{i-N} H X_{i-N}) \\ t_{i,i+1} = (\bar{\kappa}_{i-N} / \bar{\kappa}_{i-N+1}) \cosh(\bar{\kappa}_{i-N} H X_{i-N}) \\ t_{i,i-N+1} = -\sinh(\bar{\kappa}_{i-N+1} H X_{i-N}) \\ t_{i,i+2} = -\cosh(\bar{\kappa}_{i-N+1} H X_{i-N}) \end{cases} \quad (\text{S14-S17})$$

$$i = 2N : \quad \begin{cases} t_{i,i-N} = (\bar{\kappa}_{i-N} / \bar{\kappa}_{i-N+1}) \sinh(\bar{\kappa}_{i-N} H X_{i-N}) \\ t_{i,i+1} = (\bar{\kappa}_{i-N} / \bar{\kappa}_{i-N+1}) \cosh(\bar{\kappa}_{i-N} H X_{i-N}) \\ t_{i,i-N+1} = \exp(-\bar{\kappa}_{i-N+1} H X_{i-N}) \end{cases} \quad (\text{S18-S20})$$

$$t_{2N+1,N+2} = 1 \quad (\text{S21})$$

and $t_{i,j} = 0$ for couples (i, j) that are not specified in eqs S7-S21. The set of linear algebraic equations S7-S21 was solved using the Newton-Raphson method¹ for the determination of the constants $A_{j=1,\dots,N+1}$ and $B_{1,\dots,N}$. In the limit of complete dissociation of the ionizable groups within the N layers of the PEM, we have $\theta_j = 0$, $\bar{\kappa}_j = \kappa$, $\beta_j = \tilde{\rho}_j$ and it may be shown that the $A_{j=1,\dots,N+1}$ and $B_{1,\dots,N}$ are given by the closed form expressions:

$$A_1 = -\sum_{k=2}^{N+1} (\tilde{\rho}_{k-1} - \tilde{\rho}_k) \exp(-\kappa H X_{k-1}) \quad (\text{S22})$$

$$\text{For } j = 2, \dots, N+1 : \quad A_j = A_1 + \sum_{k=2}^j (\tilde{\rho}_{k-1} - \tilde{\rho}_k) \cosh(\kappa H X_{k-1}) \quad (\text{S23})$$

$$B_1 = 0 \quad (\text{S24})$$

$$\text{For } j = 2, \dots, N : \quad B_j = -\sum_{k=2}^j (\tilde{\rho}_{k-1} - \tilde{\rho}_k) \sinh(\kappa H X_{k-1}). \quad (\text{S25})$$

II. Hydrodynamics.

In the limiting case where the PEM consists of N homogeneous layers, each characterized by a given hydrodynamic softness $\lambda_j = (k_j / \eta)^{1/2}$, the Brinkman equation (eq 10 in the main text) may be rewritten for $X_{j-1} \leq X \leq X_j$ with $j = 1, \dots, N+1$ in the form:

$$\frac{d^2 V_j(X)}{dX^2} - (\lambda_j H)^2 V_j(X) = -1, \quad (\text{S26})$$

where $V_{j=1,\dots,N}(X) = V(X_{j-1} \leq X \leq X_j)$ is the dimensionless velocity distribution across the j th-layer of the PEM and V_{N+1} refers to that in the electrolyte solution (outside the PEM) where there is no friction exerted on the fluid flow, *i.e.* $\lambda_{N+1} = 0$. The solution of eq S26 is given by:

For $X_{j-1} \leq X \leq X_j$ and $j = 1, \dots, N$:

$$V_j(X) = D_j \sinh(\lambda_j H X) + E_j \cosh(\lambda_j H X) + 1/(\lambda_j H)^2 \quad (\text{S27})$$

For $X_N \leq X$:

$$V_{N+1}(X) = -X^2/2 + X/2 + D_{N+1} \quad (\text{S28})$$

where $D_{j=1,\dots,N+1}$ and $E_{j=1,\dots,N}$ are unknown constants to be determined from the boundaries specified in the main text together with conditions ensuring continuity of velocity and shear stress at the positions $X = X_{j=1,\dots,N}$. Similarly to the electrostatic problem, it is shown that the constants

$D_{j=1,\dots,N+1}$ and $E_{j=1,\dots,N}$ are solutions of the matricial equation:

$$U \cdot \vec{S}_{\text{Hyd}} = \vec{C}_{\text{Hyd}}, \quad (\text{S29})$$

where \vec{S}_{Hyd} and \vec{C}_{Hyd} are the $2N+1$ column vectors defined by:

$$\vec{S}_{\text{Hyd}} = \begin{pmatrix} D_1 \\ D_2 \\ \vdots \\ D_N \\ D_{N+1} \\ E_1 \\ E_2 \\ \vdots \\ E_N \end{pmatrix}, \quad \vec{C}_{\text{Hyd}} = \begin{pmatrix} 1/(\lambda_2 H)^2 - 1/(\lambda_1 H)^2 \\ 1/(\lambda_3 H)^2 - 1/(\lambda_2 H)^2 \\ \vdots \\ 1/(\lambda_N H)^2 - 1/(\lambda_{N-1} H)^2 \\ -X_N^2/2 + X_N/2 - 1/(\lambda_N H)^2 \\ 0 \\ \vdots \\ 0 \\ -X_N + 1/2 \\ -1/(\lambda_1 H)^2 \end{pmatrix} \quad (\text{S30,S31})$$

and U the $(2N+1) \times (2N+1)$ Jacobian matrix with elements $u_{i,j}$ given by:

$$i = 1, \dots, N-1: \quad \begin{cases} u_{i,i} = \sinh(\lambda_i H X_i) \\ u_{i,i+N+1} = \cosh(\lambda_i H X_i) \\ u_{i,i+1} = -\sinh(\lambda_{i+1} H X_i) \\ u_{i,i+N+2} = -\cosh(\lambda_{i+1} H X_i) \end{cases} \quad (\text{S32-S35})$$

$$i = N: \quad \begin{cases} t_{i,i} = \sinh(\lambda_i H X_i) \\ t_{i,i+N+1} = \cosh(\lambda_i H X_i) \\ t_{i,i+1} = -1 \end{cases} \quad (\text{S36-S38})$$

$$i = N+1, \dots, 2N-1 : \quad \begin{cases} u_{i,i-N} = (\lambda_{i-N} / \lambda_{i-N+1}) \cosh(\lambda_{i-N} H X_{i-N}) \\ u_{i,i+1} = (\lambda_{i-N} / \lambda_{i-N+1}) \sinh(\lambda_{i-N} H X_{i-N}) \\ u_{i,i-N+1} = -\cosh(\lambda_{i-N+1} H X_{i-N}) \\ u_{i,i+2} = -\sinh(\lambda_{i-N+1} H X_{i-N}) \end{cases} \quad (\text{S39-S42})$$

$$i = 2N : \quad \begin{cases} t_{i,i-N} = (\lambda_{i-N} H) \cosh(\lambda_{i-N} H X_{i-N}) \\ t_{i,i+1} = (\lambda_{i-N} H) \sinh(\lambda_{i-N} H X_{i-N}) \end{cases} \quad (\text{S43-S44})$$

$$t_{2N+1,N+2} = 1 \quad (\text{S45})$$

and $u_{i,j} = 0$ for couples (i, j) which are not specified in eqs S32-S45. The set of linear algebraic eqs S32-S45 was solved using Newton-Raphson method¹ for determination of the constants $D_{j=1,\dots,N+1}$ and $E_{1,\dots,N}$. In the limit where $\omega_{j,N} = (\lambda_j / \lambda_N)^2 = 1$ for $j = 1, \dots, N$, it is verified that the velocity field profiles given by eqs S27-S45 agree with those obtained from the analytical expression for $V(X)$ derived in our previous work on electrokinetics of monolayered film (eqs

7-8 in Reference [2] with replacing therein the quantities λ_0 and d by λ_N and $\sum_{j=1}^N \delta_j$, respectively).²

III. Electrokinetics.

Within the Debye-Hückel framework which is valid for sufficiently low electrostatic potentials $y(X)$ in line with the linearized form of the Poisson Boltzmann equation (eq S1), the streaming current I_{str} for PEM consisting of homogenous layers can be written as:

$$I_{\text{str}} / \Delta P = \sigma \left\{ \sum_{j=1}^N \int_{X_{j-1}}^{X_j} V_j(X) y_j(X) dX + \int_{X_N}^{\infty} V_j(X) y_j(X) dX \right\}, \quad (\text{S46})$$

where $\sigma = 4\ell F c^\infty H^3 / (\eta L_0)$ and the spatial profiles $y_{j=1,\dots,N+1}(X)$ and $V_{j=1,\dots,N+1}(X)$ are defined in §I (eqs S2-S3) and §II (eqs S27-S28), respectively. Equation S46 is the limiting

form of eq 11 in the main text for $\alpha_{j=1,\dots,N} \rightarrow 0$, $z_{l=1,\dots,M} = z$ and $y(X) \ll 1$. The second term in the right hand side of eq S46 stems from the contribution to the streaming current of mobile net charge in the electrolyte solution. Because we tackle practical situations with large separation distances between the two surfaces ($\kappa H \gg 1$, *i.e.* there is no overlap of electric double layers in the electrokinetic cell), the upper bound of the integral in eq 11 of the main text may be replaced by infinity. With the here-adopted nomenclature where the space variable x is adimensionalized with respect to H , we show after evaluation of the integrals involved in eq S46 that $I_{\text{str}} / \Delta P$ is provided by the full expression:

$$I_{\text{str}} / \Delta P = \sigma \left\{ A_{N+1} \frac{\exp(-\kappa H X_N)}{(\kappa H)^3} \left[D_{N+1} (\kappa H)^2 + \kappa H / 2 - (\kappa H X_N)^2 / 2 + X_N (\kappa H)^2 / 2 - \kappa H X_N \right] + \sum_{j=1}^N \{Q_j(X_j) - Q_j(X_{j-1})\} + \sum_{k=1}^4 \sum_{j=1}^N v_{k,j} \{I_{k,j}(X_j) - I_{k,j}(X_{j-1})\} \right\} \quad (\text{S47})$$

where the functions $I_{k,j}(X)$, $Q_j(X)$ and the scalars $v_{k,j}$ are defined by:

$$\left\{
\begin{aligned}
I_{1,j}(X) &= \frac{1}{2(\bar{\kappa}_j H + \lambda_j H)} \cosh[(\bar{\kappa}_j H + \lambda_j H) X] + \frac{1}{2(\bar{\kappa}_j H - \lambda_j H)} \cosh[(\bar{\kappa}_j H - \lambda_j H) X] \\
I_{2,j}(X) &= \frac{1}{2(\bar{\kappa}_j H + \lambda_j H)} \sinh[(\bar{\kappa}_j H + \lambda_j H) X] - \frac{1}{2(\bar{\kappa}_j H - \lambda_j H)} \sinh[(\bar{\kappa}_j H - \lambda_j H) X] \\
I_{3,j}(X) &= \frac{1}{2(\bar{\kappa}_j H + \lambda_j H)} \sinh[(\bar{\kappa}_j H + \lambda_j H) X] + \frac{1}{2(\bar{\kappa}_j H - \lambda_j H)} \sinh[(\bar{\kappa}_j H - \lambda_j H) X] \\
I_{4,j}(X) &= \frac{1}{2(\bar{\kappa}_j H + \lambda_j H)} \cosh[(\bar{\kappa}_j H + \lambda_j H) X] - \frac{1}{2(\bar{\kappa}_j H - \lambda_j H)} \cosh[(\bar{\kappa}_j H - \lambda_j H) X] \\
Q_j(X) &= \frac{1}{(\bar{\kappa}_j H)(\lambda_j H)^2} [A_j \sinh(\bar{\kappa}_j H X) + B_j \cosh(\bar{\kappa}_j H X)] + \frac{\beta_j}{(\lambda_j H)^2} X + \\
&\quad \frac{\beta_j}{\lambda_j H} [D_j \cosh(\lambda_j H X) + E_j \sinh(\lambda_j H X)] \\
v_{1,j} &= B_j E_j \\
v_{2,j} &= B_j D_j \\
v_{3,j} &= A_j E_j \\
v_{4,j} &= A_j D_j
\end{aligned}
\right. \tag{S48-S56}$$

IV. Supporting Figures.

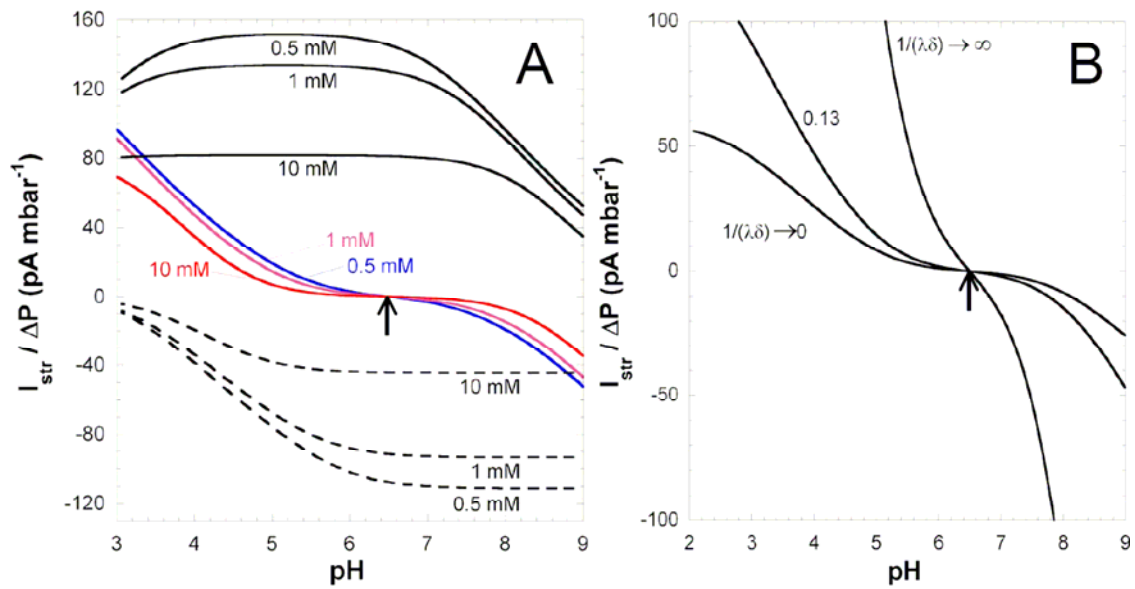


Figure S1. (A) Ratio between streaming current (I_{str}) and applied pressure (ΔP) versus pH as evaluated at three electrolyte concentrations (indicated) for a polycationic layer (black solid lines), polyanionic layer (black dotted-lines) and a soft thin-film of thickness $\delta = \delta_1 + \delta_2$, hydrodynamic softness $\lambda = \lambda_2$ where the positive and negative charges of the aforementioned polycationic and polyanionic layers are uniformly distributed. Model parameters: $pK_{a,1} = 9$, $\varepsilon_1 = +1$, $\delta_1 = 30$ nm, $pK_{a,2} = 4$, $\varepsilon_2 = -1$, $\delta_2 = 5$ nm, $n_2 = 20$ mM, $1/\lambda_2 = 4.5$ nm, $|\gamma_{1,2}| = 1$, $\omega_{1,2} = 1$ and $\alpha_{j=1,2} \rightarrow 0$. (B) As in panel A but $I_{\text{str}} / \Delta P$ vs. pH is shown for various values of $1/(\lambda\delta)$ (indicated) in 1 mM electrolyte concentration.

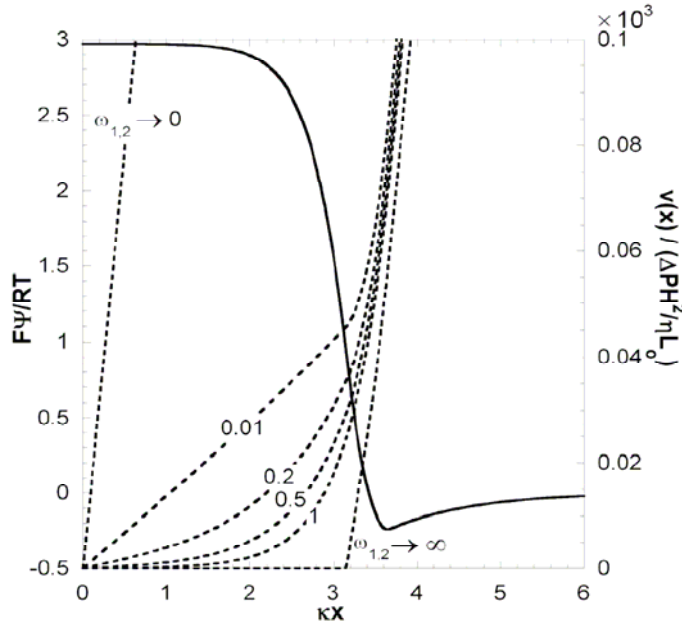


Figure S2. Distribution of dimensionless electrostatic potential (solid line) and velocity field (dotted-lines) across a bilayer film at $\text{pH} = 5.45$, $c = 1$ mM for various values of the ratio $\omega_{1,2} = k_1/k_2 = (\lambda_1/\lambda_2)^2$ for the bilayer film whose further characteristics are detailed in Figure 3B of the main text.

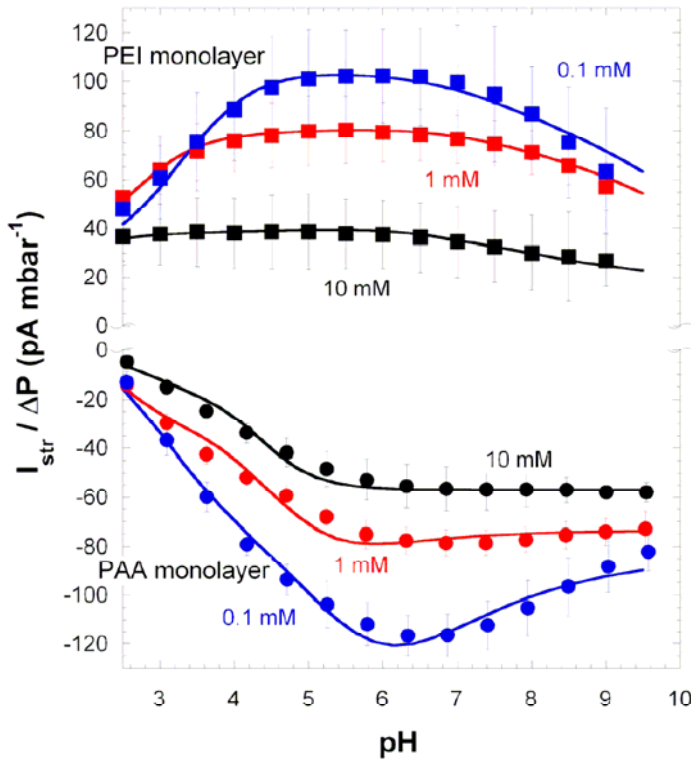


Figure S3. Symbols: ratio between streaming current (I_{str}) and applied pressure (ΔP) versus pH as measured at three electrolyte concentrations (indicated) for PEI and PAA monolayers (indicated). Solid lines: fits to theory detailed in References [2] and [3]. These data are extracted from Reference [4] where details on thickness and swelling properties of PEI and PAA monolayers can be found.

References.

1. Press, W.H.; Teukolsky, S.A.; Vetterling, W.T.; Flannery, B.P. in *Numerical recipes in Fortran, The Art of Scientific Computing*, 2nd ed.; Cambridge University Press: New-York, 1986.
2. Duval, J. F. L.; Zimmermann, R.; Cordeiro, A.L.; Rein, N. and Werner, C. *Langmuir* **2009**, *25*, 10691-10703.
3. Zimmermann, R.; Kuckling, D.; Kaufmann, M.; Werner, C. and Duval, J. F. L. *Langmuir* **2010**, *26*, 18169-18181.
4. Duval, J. F. L.; Küttner, D.; Nitschke, M.; Werner, C.; Zimmermann, R. Interrelations between charging, structure and electrokinetics of nanometric polyelectrolyte films. *J. Colloid Interface Sci.* doi:10.1016/j.jcis.2011.06.063, in press.